



Interplay between synaptic delays and propagation delays in neural fields equations

Romain Veltz

► To cite this version:

Romain Veltz. Interplay between synaptic delays and propagation delays in neural fields equations. [Research Report] 2013. hal-00780444v1

HAL Id: hal-00780444

<https://inria.hal.science/hal-00780444v1>

Submitted on 24 Jan 2013 (v1), last revised 17 Jun 2013 (v2)

HAL is a multi-disciplinary open access archive for the deposit and dissemination of scientific research documents, whether they are published or not. The documents may come from teaching and research institutions in France or abroad, or from public or private research centers.

L'archive ouverte pluridisciplinaire **HAL**, est destinée au dépôt et à la diffusion de documents scientifiques de niveau recherche, publiés ou non, émanant des établissements d'enseignement et de recherche français ou étrangers, des laboratoires publics ou privés.



Interplay between constant delays and propagation delays in neural fields equations

Romain Veltz

**RESEARCH
REPORT**

N° 8020

Janvier 2013

Project-Team NeuroMathComp



Interplay between constant delays and propagation delays in neural fields equations

Romain Veltz*

Project-Team NeuroMathComp

Research Report n° 8020 — Janvier 2013 — 46 pages

Abstract: Neural fields equations describe the activity of neural populations at a mesoscopic level. Although the early derivation of these equations introduced space dependent delays coming from the finite speed of signal propagation along axons, there has been few studies concerning their role in shaping the dynamics of neural activity. This is mainly due to the lack of analytical tractable models. On the other hand, constant delays have to be introduced to model the synaptic transmission and the spike initiation dynamics. By incorporating the two kind of delays in the neural fields equations, we are able to find the Hopf bifurcation curves analytically as well as the normal forms of the main bifurcations. This allows an in-depth study of two different types of connectivity that reveals a surprisingly rich dynamical portrait because the connectivity and the space dependent delays couple dynamically. In particular, the shape of the connectivity strongly influences the spatiotemporal dynamics.

Key-words: Neural fields equations, space-dependent delays, propagation delays, constant delay, non-uniform delay, bifurcation theory, center manifold, functional differential equations, equivariant bifurcation, Hopf-Hopf interaction, wave, mixed-mode solution.

This research was partially supported by the European Union Seventh Framework Programme (FP7/2007-2013) under grant agreement no. 269921 (BrainScaleS) and by the ERC advanced grant NerVi no. 227747.

* CNL-S, Salk Institute and NeuroMathComp team.

**RESEARCH CENTRE
SOPHIA ANTIPOLIS – MÉDITERRANÉE**

2004 route des Lucioles - BP 93
06902 Sophia Antipolis Cedex

Effets associés a la presence de délais constants et de délais de propagation dans les équations de masses neurales.

Résumé : Les équations de masses neurales décrivent l'activité de populations neurales au niveau mésoscopique. Bien que les délais de propagation, issus de la vitesse de propagation finie des signaux le long des axones, aient été incorporés dans les premières équations, il y a peu d'études concernant leur rôle dans l'établissement de l'activité neurale. Cela est principalement lié au manque de modèles analytiques. D'un autre côté, les délais constants ont été introduits pour modéliser la transmission synaptique et la dynamique de l'initiation du potentiel d'action. En prenant en compte ces deux types de délais dans les équations de masses neurales, nous donnons des formules analytiques pour les courbes de bifurcation de Hopf ainsi que pour les coefficients de différentes formes normales. Ces formules permettent une étude en profondeur de deux types de connectivités qui révèle une dynamique extrêmement riche liée au fait que la connectivité et les délais, fonctions de l'espace, se couplent de façon dynamique. Ainsi, la forme de la connectivité affecte fortement la dynamique.

Mots-clés : Equations des masses neurales, délais dépendant de l'espace, délais de propagation, délais constants, théorie des bifurcations, variété centrale, équations différentielles fonctionnelles, bifurcations équivariantes, interaction Hopf-Hopf, ondes.

1 Introduction

The Hodgkin-Huxley equations [HH52] provide an accurate and mathematically tractable description of the behavior of an individual neuron in isolation, which later formed the foundation for mesoscopic descriptions of neural networks where the fine properties of the neurons do not play a fundamental role. The neural field models [WC73, Ama77, Co05], which describe the firing rate evolution of spatially extended populations of neurons have been used successfully to model the rat barrel cortex [PBS+96] and the visual cortex [BYBOS95, MIGJ10]. More specifically, neural field models have been used to study both stationary and oscillatory behaviors; in both regimes the connectivity between neurons dictates the possible cortical states (see [EC79] for the oscillatory regime). The stationary regime has been used to describe neural hallucinations as spontaneous cortical activity [BBC00, BCG+01]. The computation of the stationary cortical states and their stability is now well documented [EC80, BBC00, BCG+01, Co05, FGS08, VF10]. An immediate question is how this stability is altered when delays are introduced. These delays arise from the finite propagation speed of signals along axons, from the synaptic time transmission, from the nonlinear spike generation mechanism or from the signal propagation in dendrites. There are a limited number of studies for which delays are taken into account but only non spatially extended populations are considered [BC94, BCVDD96, Wu98, SC00, Wu01, CL09]. Here, we use bifurcation theory to study both stationary and oscillatory behaviors in a spatially extended system with space dependent delays.

Moving from a description of neural activity by ordinary differential equations (ODEs) to delay differential equations (DDEs) requires significantly more complex mathematical and numerical tools, mainly due to the fact that the phase space becomes infinite dimensional [Wu98, HL93, Die95, ST01]. This explains the small number of studies of mesoscopic models with delays. Indeed, whenever possible, one should try to find a description of the biophysical behaviors with ordinary differential equations. However, in the case of propagation (spatially dependent) delays, there is no way to give an accurate description of the dynamics with a reduction to ODEs. Still, it would be advantageous to use equations that intrinsically contain finite propagation speeds (like the wave equation) instead of neural field equations. When the spatial connectivity is homogeneous, one can find a partial differential equation which approximates the delayed neural field equations [CVS+07] ; a major advantage of this approach is the speed-up in the numerical computation. However this advantage has been recently superseded by the algorithm in [HR10] where the authors take advantage of the convolutional structure of the homogeneous connectivities to efficiently compute the solutions of delayed neural field equations (DNFEs). To conclude, no simplification exists for general connectivities which suggests that a description of propagation delays with delay differential equations is still satisfactory.

In the approximation of networks of spiking neurons by neural field equations, it has recently been shown that constant delays must be incorporated in the mesoscopic description in order to produce oscillations - travelling waves or standing waves - observed in spiking neural networks [RBH05, RM11]. These constant delays take into account the finite integration time of the pre-synaptic action potentials by synapses. The space dependent delays coming from the finite velocity of action potentials propagating along axons are thought to play an important role in the long range connections observed in the visual cortex [Bre03, LAB03].

The linear stability of stationary cortical states of delayed neural field equations was studied in [AH05, AH06, BK08, CVS+07, Hut09, Hut08, JK00, BL10] and delay dependent/independent stability bounds were given in [AH05, AH06, HA06, Hut08, VF11]. Due largely to the fact that the eigenvalue problem is infinite dimensional, the computation of the stability has been confined to some very particular cases. Hence, little is known about the impact of (space dependent) delays on the stability of equilibria. Due to the high computational cost (even for

one dimensional cortices with homogeneous connectivities), an in-depth analysis of the values of delays and connectivity properties giving rise to oscillatory behavior has yet to be produced. Despite this limitation, the nonlinear stability has been studied in two papers [RM11, VCM07]. The first reference gives, by means of a numerical investigation of the eigenvalue problem, an almost complete description of the linear stability for constant delays; we show here that it can be done analytically in the most general case. Notice that the nonlinear analysis is done using weakly nonlinear analysis. The second reference [VCM07] applies the weakly nonlinear analysis techniques to produce simplified equations from which the stability is studied. They were able to compute the normal form of the Hopf bifurcation for different neural field models including neuronal adaptation. From a mathematical point of view, the method produces nonlinear partial differential equations for the reduced equation which are not so straightforward to study in practice; the authors consider infinite cortices, modeled in effect as the real line. By looking at bounded cortices (as in [RM11]), we show that our method produces ordinary differential equations whose normal forms are well-documented in [GH83, Kuz98, HI10]. Also, the main drawback of the use of the weakly nonlinear expansion is that the link between the dynamics of approximation and the dynamics of the full system has not been proven. We decide to apply center manifold and normal form theories in order to get around this difficulty. We recently developed such a formalism for DNFE in [VF12] based on the results in [VI92] and the general theory in [HL93].

What we would like to do here, is to understand how the space-dependent delays impact the dynamics. Indeed, little is known on the relative roles of constant delays and space dependent delays on the cortical dynamics. To this end, we apply the tools developed in [VF12] to a scalar neural field model for which the analytical computations can be pushed sufficiently far. Hence, we start with an analytical expression of the Hopf bifurcation curves in Section 4. Then, we compute, in Section 5, the normal forms of the main bifurcations that appear in the bifurcation diagrams. As a first numerical application, we look at the Mexican-hat connectivity in Section 6.1. Indeed, many of the neural field models operate near a static bifurcation point and the bifurcation can be changed into a steady state/Hopf bifurcation point or a Bogdanov-Takens bifurcation point by the introduction of delays [BYBOS95, BCG⁺01]. This has only been studied for point neurons in [CY08], which motivates further the need to compute these bifurcation points in order to understand the effect of the delays. The second numerical application given in Section 6.2 deals with the inverted Mexican-hat connectivity which produces a much richer dynamics than the first application. There are two ways of writing these paper depending on whether we want to stay at the same level of formalism as in [VF12]. We chose not to do so in order to broaden the possible audience for this work. Nevertheless, we use in the appendix the same tools as in [VF12] so that the computation of the normal forms do not suffer from a lack of rigor.

The reader not interested in the mathematical details can go directly to the numerical applications in Section 6.

2 The neural field model

Our starting point is the neural field equations that were first derived by Wilson and Cowan in [WC73] and Amari in [Ama77]. These equations describe the mean membrane potential (1) or the mean neural activity (2) (see [Erm98] for a review). They were recently heuristically related to spiking neural networks in [RBH05, RM11] where it was shown that by incorporating constant synaptic delays in neural field equations, we can recover activity of the spiking networks that was not otherwise captured. In this work, we focus on one neural population located on

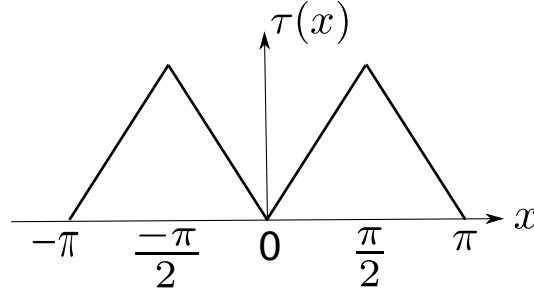


Figure 1: Plot of the periodic delay function, the saw-function.

a one-dimensional cortex $[-\frac{\pi}{2}, \frac{\pi}{2}]$ with periodic boundary conditions. Hence, for each spatial location x , the quantity $V(x, t)$ is a scalar which satisfies:

$$\begin{cases} \left(\frac{d}{dt} + l\right)V(x, t) = \int_{-\pi/2}^{\pi/2} J(x-y)S_0[\sigma V(y, t - \tau(x-y))]dy + I_{ext}(x, t), & t \geq 0 \\ V_0(x, t) = \phi(x, t), & t \in [-\tau_m, 0], x \in [-\frac{\pi}{2}, \frac{\pi}{2}] \end{cases} \quad (1)$$

where ϕ is the initial condition. The scalar l^{-1} is a time constant describing the decay of the membrane potential and the connectivity $J(x-y)$ describes how the neural population located at x is connected to the neural population at location y . We suppose that J is an *even* function and that it is π -periodic to respect the cortex topology. The sigmoid non-linearity S_0 relates the membrane potential to the firing rate $S_0(V)$. The nonlinear gain σ and the threshold are additional parameters used to describe the nonlinearity that we center at $V = 0$ to simplify the study:

$$S_0(V) = S(V - h) - S(-h), \quad S(x) = \frac{1}{1 + e^{-x}}.$$

Also, an input term I_{ext} is added to describe the sensory pathway or the input from other cortical areas. For the purpose of this work where we study spontaneous neural activity, we suppose that this input is zero, $I_{ext} = 0$, so that $V = 0$ is a stationary solution of (1). This study is devoted to the stability of the solution $V = 0$. Finally, the delay function $\tau(x-y)$ models the time D (see [RBH05]) it takes for the signal to pass through the synapses and the time $c|x-y|$ to propagate along axons where c is the inverse of the propagation speed. Note that we suppose implicitly that axons are straight lines with this last delay term. This assumption is based on [BKF⁺10] and does not alter the generality of our study. We also suppose that the delays are a π -periodic function of space so that:

$$\tau(x, y) = D + c|x-y|_\pi \equiv \tau(x-y)$$

as shown in Figure 1 where $|\cdot|_\pi$ is the π -periodic absolute function. It is useful for the rest of our study to define the maximum delay:

$$\tau_m \equiv \max \tau = D + c\frac{\pi}{2}.$$

In the following, we compute the bifurcation diagrams for any connectivity function J . However, only a nonlinear analysis will provide the stability of the bifurcating patterns as traveling/standing waves for example. To this end, having a small number of parameters is a necessity. A simple way to lower the number of parameters is to impose symmetries to the model as we

did: for example, it requires one parameter (*i.e.* the spatial extension) to describe a rotation invariant 2D connectivity with a Gaussian whereas it would require more parameters to break this symmetry. However, there is a price to pay for having less parameters by assuming symmetries: the normal forms are more complex and not always tabulated.

Finally, we would like to give the equations for the activity-based model although we will not study it here.

$$\left(\frac{d}{dt} + l\right)A(x, t) = S_0 \left[\sigma \int_{-\pi/2}^{\pi/2} J(x - y)V(y, t - \tau(x - y))dy + \sigma I_{ext}(x, t) \right]. \quad (2)$$

Indeed, if the two models (1) and (2) display the same bifurcation points, their normal forms are different. Hence, they produce different dynamics even if the parameters are the same. The computation of the normal forms in the case of the potential based model (1) is already a daunting task so that we focus on this particular model here.

3 Mathematical framework and notations

The equations (1) feature delay differential equations on the space of periodic functions that are square integrable $\mathcal{F} \equiv L^2\left(\left[-\frac{\pi}{2}, \frac{\pi}{2}\right], \mathbb{R}\right)$ endowed with the scalar product

$$\langle U, V \rangle_{L^2} \equiv \int_{-\pi/2}^{\pi/2} U(x)V(x)dx.$$

Given any initial condition in $C^0([-\tau_m, 0], \mathcal{F})$, there is a unique solution to (1). We proved in [VF11] that there is a global attractor so that the dynamics cannot explode.

Let us now introduce notations. The history segment V_t is the function $V_t : \theta \rightarrow V(t + \theta, \cdot)$ for $\theta \in [-\tau_m, 0]$, it belongs to $C^0([-\tau_m, 0], \mathcal{F})$. In a way, delay differential equations are evolution equations for time-window vectors V_t . Hence, the phase space, also called the *history space*, is made of functions V_t from $[-\tau_m, 0]$ to \mathcal{F} . The delay term is encoded in the linear operator

$$L_1 : \phi \rightarrow \int_{-\pi/2}^{\pi/2} J(\cdot - y)\phi(y, -\tau(\cdot - y))dy$$

so that the equations (1) can be compactly written:

$$\begin{cases} \dot{V}(t) = -lV(t) + {}_1S_0(V_t) \\ V_0 = \phi \end{cases}$$

Note that $V = 0$ is an equilibrium of (1): we are interested in the patterns that bifurcate from this equilibrium. Recall that (1) has a Lyapunov functional when $\tau = 0$ and that all trajectories are bounded. Hence, we cannot find non-constant periodic orbits when $\tau = 0$.

Let us introduce some basic tools of equivariant bifurcation theory which can be found, for example, in [GSS88, CL00, HI10]. Note that (1) is $O(2)$ -equivariant with respect to the following action which means that the action commutes with the righthand side of (1):

$$\forall \phi \in C^0([-\tau_m, 0], \mathcal{F}), \quad \begin{cases} (R_\gamma \cdot \phi)(\theta, x) = \phi(\gamma + x, \theta) \\ (S \cdot \phi)(\theta, x) = \phi(-x, \theta). \end{cases}$$

It is easy to see that the group generated by R_γ, S is indeed isomorphic to $O(2)$. The fact that (1) commutes with the translations R_γ follows from the convolution involving the connectivity J . Also the equivariance *w.r.t.* the reflection S comes from J being an even function.

In the following, we use the notations $\cos_n(x) = \cos(2nx)$, $\sin_n(x) = \sin(2nx)$ and $e_n(x) = e^{2inx}$. Also $(f)_n \equiv \int_{-\pi/2}^{\pi/2} f \cos_n$ written f_n when possible. It is useful to note that if J is even, then $J \cdot e_n = (J)_n e_n$.

Finally, we will write s_k the derivative of the nonlinearity S_0 at 0

$$s_k \equiv S^{(k)}(0).$$

4 Linear analysis

In this section, we study the asymptotic stability of $V = 0$ by means of the *characteristic values* that we define as follow. The linearization of (1) around the stationary solution $V = 0$ gives:

$$\frac{d}{dt}U(x, t) = -lU(x, t) + \sigma s_1 \int_{-\pi/2}^{\pi/2} J(x-y)U(y, t - \tau(x-y))dy \quad (3)$$

Looking at exponential perturbations $U(x, t) = U(x)e^{\lambda t}$, we find that $U(x)$ solves the characteristic equation:

$$(\Delta(\lambda)U)(x) \equiv \lambda U(x) + lU(x) - \sigma s_1 e^{-\lambda D} \int_{-\pi/2}^{\pi/2} J(x-y)e^{-\lambda c|x-y|\pi} U(y)dy = 0.$$

The solutions $U(x)$ of this linear equation are $\sin(2nx), \cos(2nx)$ so that the *characteristic values* λ solve

$$\lambda + l - \sigma s_1 e^{-\lambda D} \left(J e^{-\lambda c|\cdot|\pi} \right)_n = 0. \quad (4)$$

where $(J e^{-\lambda c|\cdot|\pi})_n$ is the Fourier transform of the function $x \rightarrow J(x)e^{-\lambda|x|\pi}$. We proved in [VF12] that $V = 0$ is asymptotically stable if and only if $\Re \lambda < 0$ for all *characteristic value* λ . Hence, we are led to solve (4) in order to study the stability of $V = 0$. More precisely, we are particularly interested in the critical characteristic values λ_c such that $\Re \lambda_c$ is maximal: we call them the rightmost characteristic values. Two cases can happen, either we have that $\lambda_c = 0$ which is called a static bifurcation, or we have $\lambda_c = \beta \omega_c$ which is a dynamic bifurcation.

The case of the static bifurcation is easy to analyze as one can easily prove that $\lambda = 0$ is a characteristic value if and only if $\exists n \mid l = s_1 J_n$, this condition does not depend on the delay τ . The case of the dynamic bifurcation is more involved and is now analyzed in detail. This will be the basis of our numerical analysis.

In [VF12], we wrote (1) as a Cauchy problem, *i.e.* as a regular ordinary differential equation, albeit in a subset of the history space $C^0([-\tau_m, 0], \mathcal{F})$ (see also Section B). We then showed that the characteristic values are the eigenvalues of the linearized vector field at the stationary solution $V = 0$. Also, the history segment $\theta \rightarrow e^{\lambda \theta} e_n$ appears to be the eigenvector associated to the eigenvalue λ . It is then legitimate, as we will do in the following, to use the word eigenvalue for characteristic value.

4.1 Hopf curve in the case of constant delays $c = 0$

We first restrict our study to the case $c = 0$. This case has been studied in [RBH05, RM11] where the authors showed that constant delays have to be introduced in neural field equations in order to explain oscillatory patterns seen in spiking networks. The characteristic equation (4) reads in this case:

$$\lambda + l - \sigma s_1 e^{-\lambda D} J_n = 0. \quad (5)$$

where J_n is the Fourier coefficient $J_n \equiv \int_{-\pi/2}^{\pi/2} J(y) \cos(2ny) dy$. The previous equation is solved using the different branches W_k of the Lambert function W (see [CGH⁺96]) which satisfies $W(z)e^{W(z)} = z$, $z \in \mathbb{C}$. It is straightforward to compute the solutions of (5):

$$\lambda_{k,n} = \frac{1}{D} W_k(D e^{lD} s_1 \sigma J_n) - l, \quad k \in \mathbb{Z}, \quad n \in \mathbb{N} \quad (6)$$

By using the proof in [Vel11], we find that the rightmost characteristic values belong to the subsequence $(\lambda_{0,n})_n$. The expression (6) was not reported in [RBH05, RM11] whereas it makes the linear analysis entirely analytical. It allows us to compute the rightmost Hopf bifurcation curves which are the set of parameters for which the rightmost characteristic value is purely imaginary.

Proposition 4.1 *A necessary and sufficient condition for the rightmost eigenvalue to be purely imaginary and nonzero is the existence of an integer n_0 such that $s_1 \sigma J_{n_0} \leq -l$ and $\arccos\left(\frac{l}{s_1 \sigma |J_{n_0}|}\right) \leq |\arg J_{n_0}|$. In this case the corresponding critical delay D_{n_0} and the eigenvalue $i\omega_{n_0}$ satisfy:*

$$lD_{n_0} = \frac{1}{\sqrt{\left(\frac{s_1 \sigma |J_{n_0}|}{l}\right)^2 - 1}} \left(\pi - \arccos\left(\frac{l}{s_1 \sigma |J_{n_0}|}\right) \right), \quad \omega_{n_0} = l \sqrt{\left(\frac{s_1 \sigma |J_{n_0}|}{l}\right)^2 - 1}$$

Proof. Straightforward adaptation of [Vel11].

It follows that, if $s_1 \sigma J_p < s_1 \sigma J_n \leq -l$, then $D_n < D_p$. Similar expressions were found for a network of neurons on a ring in [CYB05]. This proposition provides some biological insights: if we analyze a network without delays, we can only make it oscillate (through a Hopf mechanism) if the inhibition is strong enough, that is if $s_1 \sigma J_n \leq -l$ for some n . This result, together with the bifurcation analysis exposed in [RM11], gives a fairly complete overview of what can happen in scalar neural field equations with constant delays.

Remark 1 These results are straightforward to generalize to more general intrinsic dynamics like $\left(\frac{d}{dt} + l\right)^2$.

4.2 Hopf curve in the case of space dependent delays

We now return to the general case $c > 0$. This problem has been studied in [CVS⁺07, VCM07, BK08]. Our approach is the following: instead of looking for parameters which produce purely imaginary characteristic values $\lambda = i\omega$, we plug $\lambda = i\omega$ into (4) and vary ω . This provides naturally a parametrization of the Hopf curve. Hence, we do not need to look for this curve in the parameter plane, we are already there. Note that this strategy works for general delay functions τ and general connectivity J (see [Vel11]). In practice the following result [Vel11] gives the rightmost Hopf curves in the parameter plane (D, c) .

Proposition 4.2 Let us define the function $J_n(z) \equiv \int_{-\pi/2}^{\pi/2} J(y) e^{-iz|y|} \cos(2ny) dy \in \mathbb{C}$ and the curves \mathcal{C}_n for $n \in \mathbb{N}$:

$$\mathcal{C}_n : \left[il\sqrt{s_1\sigma|J_n(z)/l|^2 - 1}, D_n(z), \frac{z}{l\sqrt{s_1\sigma|J_n(z)/l|^2 - 1}} \right], \quad iz \in \mathcal{E}_n \quad (7)$$

where $lD_n(z) = \frac{1}{\sqrt{s_1\sigma|J_n(z)/l|^2 - 1}} \left(|\arg(J_n(z))| - \arccos\left(\frac{l}{s_1\sigma|J_n(z)|}\right) \right)$ and

$$iz \in \mathcal{E}_n = \left\{ iz \in i\mathbb{R}_+ \mid \Im J_n(z) > 0, \quad l \leq s_1\sigma|J_n(z)| \text{ and } \arccos\left(\frac{l}{s_1\sigma|J_n(z)|}\right) \leq |\arg(s_1\sigma J_n(z))| \right\}.$$

1. A necessary and sufficient condition for an eigenvalue to be purely imaginary and nonzero is the existence of an integer n_0 such that $(i\omega_0, D, c)$ belongs to the curve \mathcal{C}_{n_0} . In this case, $i\omega_0$ is an eigenvalue.
2. If we look for solutions $(i\omega, D, c)$ with $c \leq c_\infty$, then the sets \mathcal{E}_n are bounded by $z \leq c_\infty s_1\sigma \|J\|_2$. c_∞ is an arbitrary upper bound on the inverse velocity.
3. The set \mathcal{E}_n is empty if $nl > s_1^2\sigma^2 \|J\|_2^2$. Hence, there are at most $\lfloor \|s_1\sigma J\|_2^2 / l \rfloor$ curves \mathcal{C}_n .

Note how this proposition is similar to proposition 4.1. In particular, once we are given a maximum delay τ_m , we can compute all the Hopf bifurcation curves in the plane (c, D) without missing any one. Step 2. is very useful as it gives a bound to compute the coefficients $J_n(z)$. The formulas are straightforward to compute in *Matlab*[®], for example. In order to avoid any numerical inaccuracy in the computation of the curve \mathcal{C}_n which come from the oscillating integrals $J_n(z)$, we use a Newton method on equation (4) with the formula (7) as an initial seed.

We will see that the Hopf curves accumulate when $c \rightarrow \infty$ so that it may be useful to plot the curves in the parameter plane $(s_1\sigma, l)$.

Corollary 4.3 The Hopf curves in the parameter space $(s_1\sigma, l)$ at (c, D) fixed are given by:

$$l(z) = \frac{z}{c} \frac{1}{\sqrt{\frac{1}{\cos\left(\frac{z}{c}D - |\arg(J_n(z))|\right)^2} - 1}}, \quad \sigma(z) = \frac{l(z)}{s_1|J_n(z)|} \sqrt{\frac{z^2}{l(z)^2 c^2} + 1} \quad (8)$$

where $z \in \mathcal{E}_n$.

Proof. Let us consider a fixed delay term τ defined by the couple (c, D) . From the formula (7), we find $\omega(z) = l\sqrt{s_1\sigma|J_n(z)/l|^2 - 1}$ and $z^2 = c^2 l^2 \left(s_1^2 \sigma^2 \frac{|J_n(z)|^2}{l} - 1 \right)$ i.e. $\sqrt{\frac{z^2}{l^2 c^2} + 1} = s_1\sigma \frac{|J_n(z)|}{l}$. From $\omega(z)D = \frac{z}{c}D = |\arg(J_n(z))| - \arccos\left(\frac{l}{s_1\sigma|J_n(z)|}\right)$, we find $\cos\left(\frac{z}{c}D - |\arg(J_n(z))|\right) = \frac{1}{\sqrt{\frac{z^2}{l^2 c^2} + 1}}$ which is solved in l . The expression for s follows from $\sqrt{\frac{z^2}{l^2 c^2} + 1} = s_1\sigma \frac{|J_n(z)|}{l}$.

5 Nonlinear analysis, normal form computation

Let us write the parameters μ and suppose that some of the rightmost eigenvalues lie on the imaginary axis for a given set of parameters μ_c . The corresponding eigenvectors span the center part \mathcal{X}_c . Then, the dynamics of (1) can be very well approximated by the dynamics restricted on an invariant and exponentially attracting center manifold which is parametrized by the finite dimensional center part. This result is called the center manifold theorem and we proved it for delayed neural field equations in [VF12]. It follows that close to a bifurcation point μ_c , the dynamics can be described by a finite number of ordinary differential equations called the *reduced equations* (see for example [HI10] and appendix B) which describe the dynamics restricted to the invariant and attracting center manifold. More precisely, we write ϕ_i the eigenvectors spanning the center part \mathcal{X}_c and consider $u_c = \sum_{i=1}^{\dim \mathcal{X}_c} z_i \phi_i + c.c.$ (complex conjugate) where z_i are complex numbers. Then, we can write ordinary differential equations in the variables z_i which are *equivalent* to (1) on the center manifold. We can study directly these equations to access the dynamics of (1) but the study can be further simplified.

Indeed, using a near identity change of variables $u_c \equiv v_0 + \Phi_\mu(v_0)$ in the z_i s, we can make a Taylor truncation of the *reduced equations*, at some given order. By removing the maximum number of monomials, we can achieve the simplest possible truncation. This procedure is called the normal form method. The structure of the normal forms associated to each bifurcation is known from symmetry arguments (see [GSS88]): they are polynomials whose coefficients need to be expressed as functions of the parameters of our model (1). However, to relate these coefficients and the model parameters, we need to find the center manifold expression and the normal form change of variables Φ_μ . Fortunately, there is a way to combine the equations for the center manifold expression and for the normal form change of variables Φ_μ in one equation as recalled in Section C. It then produces equations that are solved in the coefficients of the normal forms.

Once this normal form has been computed, we can analyze it to predict behaviors in the full model (1) as function of the different parameters. In the following, we give the expression of the main normal forms that show up in our numerical experiments and we derive their dynamical properties. The expression of their coefficients is given in the appendix.

We wish to make an important technical remark on which parameters we are allowed to use in the computation of the normal forms. The nonlinearity must be regular enough with respect to these parameters and this can be an issue for the parameters c and D for two reasons. The first reason is that the history space is changing (it changes the maximum delay τ_m) and the second is the lack of regularity of the righthand side of (1). In the case where only one of these parameters is non-zero, then we can rescale time and extract the delay parameter. For example, if¹ $D = 0$, then the time rescaling $t \rightarrow t/c$ yields

$$\frac{d}{dt}V(x, t) = c \left(-lV(x, t) + \int_{-\pi/2}^{\pi/2} J(x - y) S_0(V(y, t - |x - y|_\pi)) dy \right)$$

and the right-hand side is regular in c . Note that the history space is fixed as the maximum time delay is then $\tau_m = \pi$. This shows that we can't take the pair (c, D) as parameters. In the following, we compute the normal forms truncated at cubic order whose expression is only dependent on the value of the parameters at the bifurcation point. Hence, at cubic order, if we are interested in other parameters, we only have to compute the terms linear in the z_i s.

¹The case $c = 0$ is analogue.

5.1 Scaling of parameters

In our following numerical experiments, the connectivity will be assumed to be $J(x) = \frac{2}{\pi}(J_0 + J_1 \cos_2)$. Up to a scaling of the nonlinear gain σ and the threshold h , we can hold J_0 constant and only vary J_1 in the bifurcation curves. This gives the set of parameters $(J_1, \sigma, h, l, D, c)$. It is obvious from the eigenvalue equation (4) that we can assume $h = 0$ by scaling the slope σ , hence the Hopf curves are computed as function of $s_1\sigma$. Finally, (4) also shows that if we have a solution $(\lambda, J_1, \sigma s_1, l, D, c)$, then so is $(\lambda/l, J_1, \sigma s_1/l, 1, lD, lc)$. Hence we can also assume $l = 1$ when computing the Hopf bifurcation curves.

5.2 The Pitchfork bifurcation

Let us assume here that \cos_n, \sin_n with $n \neq 0$, are in the two-dimensional null-space of $\Delta(0) = l\text{Id} - \sigma s_1 J$ at the value $\sigma_P = \frac{l}{s_1 J_n}$ of σ . We write the change of coordinates $v_0 = ze_n + c.c.$ (complex conjugate) with $z \in \mathbb{C}$. We chose σ as the bifurcation parameter, this choice only affects the expression of $a_n^{(P)}\tilde{\sigma}$ in (9). In the non-delayed case, the normal form is (see [GSS88, CE04, RM11]):

$$\dot{z} = \frac{l}{\sigma_P} \tilde{\sigma} z + \chi_n z |z|^2 + o(z^3)$$

with $\sigma = \sigma_P + \tilde{\sigma}$ and $\chi_n = \sigma_P^3 J_n \left[\frac{s_3}{2} + \sigma_P s_2^2 \left(\frac{J_0}{1-J_0/J_n} + \frac{J_{2n}}{2(1-J_{2n}/J_n)} \right) \right]$. From [GS85, HI10], the normal form in the delayed case has the same structure:

$$\dot{z} = a_n^{(P)} \tilde{\sigma} z + b_n^{(P)} z |z|^2 + o(z^3) \quad (9)$$

with $b_n^{(P)} = \pi \bar{\beta} \chi_n$, $a_n^{(P)} = \pi \bar{\beta} \frac{l}{\sigma_P}$ (see lemma E.1 for the computation) where

$$\bar{\beta}^{-1} = \pi (1 + \sigma_P s_1 (J\tau)_n) \quad (10)$$

is real. Hence, only a time scaling changes the normal form after the introduction of delays. Depending on the sign of $(J\tau)_n$, the value of $\pi \bar{\beta}$ is greater or smaller than 1. Hence, the local dynamics are slowed down or sped up by the introduction of delays.

5.3 The O(2)-Hopf bifurcation

It is known that in the non-delay case ($\tau = 0$), the network (1) does not support periodic solutions; this is not the case with delays. Suppose that there is a simple eigenvalue $i\omega_H$ and $n \neq 0$ (but see remark 2) when the parameters (D, c) are equal to (D_H, c_H) . We write τ_H the delay function $D_H + c_H| \cdot |_\pi$. Then a Hopf bifurcation with $O(2)$ symmetry arises at (D_H, c_H) . This bifurcation is described in [GS85, HI10]. By definition, we have $\Delta(i\omega_H)e_n = 0$ and the eigenvectors read: $\phi_1 = e^{i\omega_H \theta} e_n$, $\phi_2 = e^{i\omega_H \theta} e_{-n}$. By using proposition D.1, we find the following condition regarding the simplicity of the eigenvalue $i\omega_H$:

$$1 + s_1 \sigma_H (J\tau_H e^{-i\omega_H \tau_H})_n \neq 0. \quad (11)$$

We define $\beta^{-1} = \pi(1 + s_1 \sigma_H (J\tau_H e^{i\omega_H \tau_H})_n)$ and assume that σ is the free parameter while τ is held constant at τ_H . In the coordinates system: $v_0 = z_1 \phi_1 + z_2 \phi_2 + c.c.$ with $z_i \in \mathbb{C}$, it is known that the normal form (see [CL00, HI10]) for the $O(2)$ -Hopf is:

$$\begin{cases} \frac{dz_1}{dt} = z_1(i\omega_H + a_n^{(H)}(\sigma - \sigma_H) + b_n^{(H)}|z_1|^2 + c_n^{(H)}|z_2|^2) \\ \frac{dz_2}{dt} = z_2(i\omega_H + a_n^{(H)}(\sigma - \sigma_H) + b_n^{(H)}|z_2|^2 + c_n^{(H)}|z_1|^2) \end{cases} \quad (12)$$

where the normal form coefficients are given in Lemma F.1 and $a_n^{(H)} = \pi \bar{\beta} \frac{i\omega_H + l}{\sigma_H}$.

Using polar coordinates $z_i = \rho_i e^{i\theta_i}$, the equations for ρ_i do not depend on θ_i and the dynamics are characterized by a planar system in (ρ_1, ρ_2) . The phase diagram of this planar system is in Figure 2. The two equilibria $(0, \rho_1^f)$, $(\rho_0^f, 0)$ correspond to *travelling waves* while the equilibrium

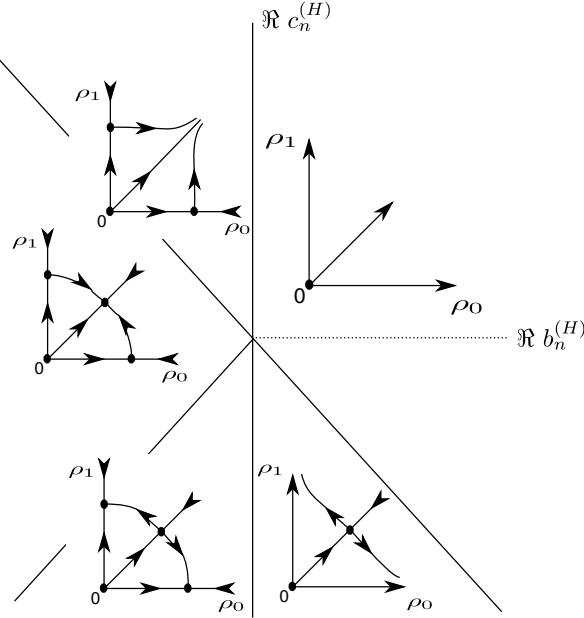


Figure 2: Phase portraits in the (ρ_0, ρ_1) plane of the equations for (ρ_0, ρ_1) , for $\Re \alpha(c - c_H) > 0$.

(ρ_0^f, ρ_1^f) corresponds to a *standing wave*. Indeed, the standing wave solution is $2\rho_0^f \Re(e^{i\omega_H t} e^{2inx} + e^{i\omega_H t} e^{-2inx}) = 4\rho_0^f \cos(\omega_H t) \cos(2nx)$ and the travelling wave solution is $2\rho_0^f \Re(e^{i\omega_H t} e^{2inx}) = 2\rho_0^f \cos(\omega_H t + 2nx)$. Thus, the dynamics at the Hopf bifurcation point is fairly simple.

Remark 2 If $n = 0$, following the same procedure, we find the normal form:

$$\frac{dz}{dt} = z(i\omega_H + a_0^{(H)}(\sigma - \sigma_H) + b_0^{(H)}|z|^2)$$

where the expression of $a_0^{(H)}, b_0^{(H)}$ is the same as the expression of $a_n^{(H)}, b_n^{(H)}$ except for the change $n \rightarrow 0$.

5.4 The Pitchfork-Hopf normal form

We suppose that the Pitchfork bifurcation curve $\sigma = \sigma_P$ intersects a Hopf bifurcation curve with frequency ω_{PH} : this gives a Pitchfork-Hopf bifurcation. We denote by σ_{PH} the value $\sigma_P = \frac{1}{s_1 J_n}$. We restrict the study to the case where the eigenvector associated to the eigenvalue $i\omega_{PH}$ is in the 0-mode e_0 and that the eigenvector for the eigenvalue 0 is in the n -mode with $n \neq 0$: this is called the 0 : n steady-state/Hopf mode interaction². This is a simple sub-case as well as the case $n : 0$. The difficult case, which we shall not study, is the case $n : p$ with n, p non zero. Note that in our numerical experiments, this latter case never happen. We write τ_{PH} the delay function

²see [GSS88] for example.

$D_{PH} + c_{PH}| \cdot |_\pi$ We chose two bifurcation parameters: (σ, l) , the other are held constant. The two eigenvectors are given by:

$$\phi_1 = e_n, \quad \phi_2 = e^{i\omega_{PH}\theta} e_0.$$

If we write $v_0 = z_1\phi_1 + z_2\phi_2 + c.c.$ with $z_1, z_2 \in \mathbb{C}$, then it is known (see [GSS88]) that the normal form does not contain any second order terms, hence it is written:

$$\begin{cases} \dot{z}_1 &= \left(a_1 + b_n^{(P)}|z_1|^2 + c_{(1)}^{(PH)}|z_2|^2 \right) z_1 \\ \dot{z}_2 &= \left(i\omega_{PH} + a_2 + b_0^{(H)}|z_2|^2 + c_{(2)}^{(PH)}|z_1|^2 \right) z_2 \end{cases} \quad (13)$$

where the complex coefficients are given in lemma G.1. Note that two coefficients $b_n^{(P)}, b_0^{(H)}$ are the same as for the Pitchfork bifurcation and the Hopf bifurcation. Hence, we only have to compute the coupling coefficients $c_{(1)}^{(PH)}, c_{(2)}^{(PH)}$. The choice of the varying parameters only affects the expression of the coefficients a_k which satisfy

$$a_1/\pi\bar{\beta}_1 = \frac{\tilde{\sigma}}{\sigma_{PH}} - \tilde{l}, \quad a_2/\pi\bar{\beta}_2 = (l_{PH} + i\omega_{PH})\frac{\tilde{\sigma}}{\sigma_{PH}} - \tilde{l}$$

where $\bar{\beta}_1^{-1} = \pi + \pi\sigma_{PH}s_1(J\tau)_n \in \mathbb{R}$, $\bar{\beta}_2^{-1} = \pi + \pi\sigma_{PH}s_1(J\tau e^{-i\omega_{PH}\tau})_0$ and $l = l_{PH} + \tilde{l}$.

Using polar coordinates $z_1 = P e^{i\phi_P}$, $z_2 = H e^{i\phi_H}$, the variables decouple and we obtain a planar system for the amplitudes:

$$\begin{cases} \dot{P} &= (\Re a_1 + \Re b_n^{(P)} P^2 + \Re c_{(1)}^{(PH)} H^2) P \\ \dot{H} &= (\Re a_2 + \Re b_0^{(H)} H^2 + \Re c_{(2)}^{(PH)} P^2) H \end{cases} \quad (14)$$

The only fixed points of this system are (see [GH83, Chapter 7.5]): $O_P = (0, \sqrt{\frac{-\Re a_2}{\Re b_0^{(H)}}})$, $O_H = (\sqrt{\frac{-\Re a_1}{\Re b_n^{(P)}}}, 0)$ and $O_{PH} = (\sqrt{-\frac{\Re a_1 \Re b_0^{(H)} - \Re c_{(1)}^{(PH)} \Re a_2}{\Delta}}, \sqrt{-\frac{\Re a_2 \Re b_n^{(P)} - \Re c_{(2)}^{(PH)} \Re a_1}{\Delta}})$ where $\Delta = \Re b_0^{(H)} \Re b_n^{(P)} - \Re c_{(1)}^{(PH)} \Re c_{(2)}^{(PH)}$.

The equilibria of (14) on the P-axis are also equilibria of (13), while the equilibria not on the P-axis are periodic orbits³ of (13). $\frac{2\pi}{\omega_0}$ -periodic solutions in the plane (P, H) are quasi-periodic⁴ solutions of (1) with two basic periods $2\pi/\omega_0, 2\pi/\omega_{PH}$ (see [GH83, chapter 7.5, page 400]). Hence, the 3 points O_P, O_H, O_{PH} correspond, to a stationary solution, to a uniformly oscillating solution and to a superposition of these two solutions respectively. Another interesting phenomenon is the possibility of the appearance of a quasi-periodic solution for (1) which is explained by the existence of a Hopf bifurcation for (14) around O_{PH} . No Hopf bifurcation can occur around O_P, O_H , however, it is possible around O_{PH} (see [LI80]) when $\Delta > 0$, $b_n^{(P)} \Re(b_0^{(H)}) < 0$.

The different phase diagrams of (14) are listed in [GH83, chapter 7]. We only show in Figure 3 the phase diagram *Ib* from [GH83, chapter 7.5, page 401] because it will appear in our numerical experiments. It features (in red) bi-stability between the stationary solution O_P and the uniformly oscillating solution O_H . The mixed-mode O_{PH} solution is never stable.

5.5 The Hopf-Hopf normal form

As we shall see in the next Section 6, the Hopf curves computed with proposition 4.2 may intersect. This intersection may involve two different Fourier modes. To keep the computations

³because we have $v_0 = 2\Re(Pe^{2inx+i\phi_P} + He^{i\omega_{PH}t+i\phi_H})$

⁴because we have $v_0 = 2\Re(P\cos(\omega_0 t)e^{2inx+i\phi_P} + H\sin(\omega_0 t)e^{i\omega_{PH}t+i\phi_H})$

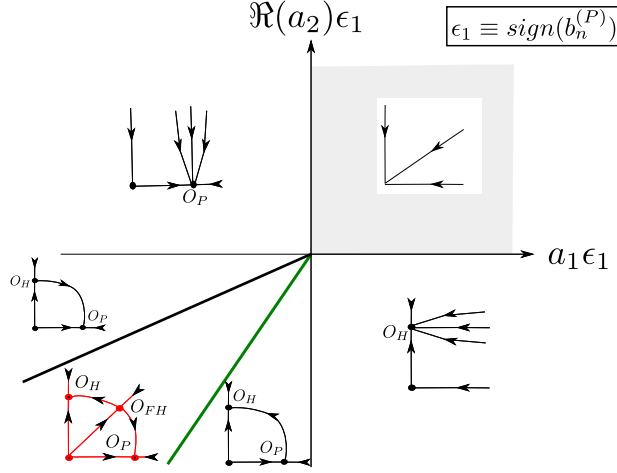


Figure 3: Phase diagram *Ib* in [GH83, chapter 7.5, page 401] with time reversal, *i.e.* in the terminology of [GH83], it corresponds to the phase diagram *Ib* for which time has been reversed. We plot here the resulting diagram. In each domain, the small phase diagram gives the corresponding dynamics for the equations (14) in the plane (P, H) . Note that the diagrams are a bit different from [GH83, chapter 7.5, page 401] because we applied the inverse scaling of [GH83, chapter 7.5, page 397].

manageable, we assume that the intersection happens between the 0-mode and the n -mode where $n > 0$: this is called the $0 : n$ Hopf-Hopf mode interaction. The more general mode interaction $p : n$ will not be considered in detail.

5.6 Six-dimensional case

This case was also studied in [RM11] for constant delays. From proposition 4.1, it is easy to see that the Hopf-Hopf bifurcation is possible for constant delays if and only if the connectivity has two Fourier modes which are equal: $J_0 = J_n$. With propagation delays, we see in Figure 12 that this is not the case here. Let us write $i\omega_0$, $i\omega_n$, the purely imaginary eigenvalues at the Hopf-Hopf point. The normal form of this bifurcation is different depending on whether or not $\frac{\omega_0}{\omega_n} \in \mathbb{Q}$ (see for example [GSS88, HI10]). It is impossible to check this hypothesis with the expressions in proposition 4.2. We will assume that $\frac{\omega_0}{\omega_n} \notin \mathbb{Q}$ and check that we are far from resonances, *i.e.* that $\frac{\omega_0}{\omega_n}$ cannot be well approximated by rationals $\frac{p}{q}$ such that $p + q < 5$. In this case the nonlinear terms of the normal form are very similar to those of the Pitchfork-Hopf normal form that we have analyzed in the previous section. The expression of the eigenvectors is the same as for the $O(2)$ -Hopf, hence

$$\phi_0 = e^{i\omega_0\theta} e_0, \quad \phi_1 = e^{i\omega_1\theta} e_n, \quad \phi_2 = e^{i\omega_1\theta} e_{-n},$$

The coordinates are $v_0 = z_0\phi_0 + z_1\phi_1 + z_2\phi_2 + c.c.$ and, from [CGK86, GSS88], the normal form reads:

$$\begin{cases} \dot{z}_0 = z_0 \left(i\omega_0 + a_0 + b_0^{(H)} |z_0|^2 + c_{(0)}^{(HH)} (|z_1|^2 + |z_2|^2) \right) \\ \dot{z}_1 = z_1 \left(i\omega_1 + a_1 + b_{(1)}^{(HH)} |z_0|^2 + b_n^{(H)} |z_1|^2 + c_n^{(H)} |z_2|^2 \right) \\ \dot{z}_2 = z_2 \left(i\omega_1 + a_1 + b_{(1)}^{(HH)} |z_0|^2 + c_n^{(H)} |z_1|^2 + b_n^{(H)} |z_2|^2 \right). \end{cases} \quad (15)$$

The expressions for the coefficients are given in lemma H.1. As before, the choice of the two varying parameters only affects the coefficients a_k . We compute the a_k s in the case $\mu = (\sigma, l)$. We find similar expressions as in the Pitchfork-Hopf bifurcation:

$$\begin{aligned} a_0/\pi\bar{\beta}_0 &= (l_{HH} + i\omega_0)\frac{\bar{\sigma}}{\sigma_{HH}} - \tilde{l} \\ a_1/\pi\bar{\beta}_1 &= (l_{HH} + i\omega_1)\frac{\bar{\sigma}}{\sigma_{HH}} - \tilde{l} \end{aligned} \quad (16)$$

Let us note that each space $\{z_0 = 0\}$ or $\{z_1 = z_2 = 0\}$ is invariant under the dynamics of (15): the dynamics are the same as in the Hopf case in the n or 0-mode. However, compared to the Hopf case, this normal form can generate superpositions of oscillatory behaviors like $(z_0(t), z_1(t), 0)$ or $(z_0(t), z_1(t), z_1(t))$ for example. More precisely, in [CGK86], all type of solutions are derived from symmetry arguments: they are only six cases, namely $(0, 0, 0)$, $(z_0, 0, 0)$, $(0, z_1, 0)$, $(0, z_1, z_1)$, $(z_0, z_1, 0)$, (z_0, z_1, z_1) and only the last two can lose stability via a Hopf bifurcation. By using the expression of our

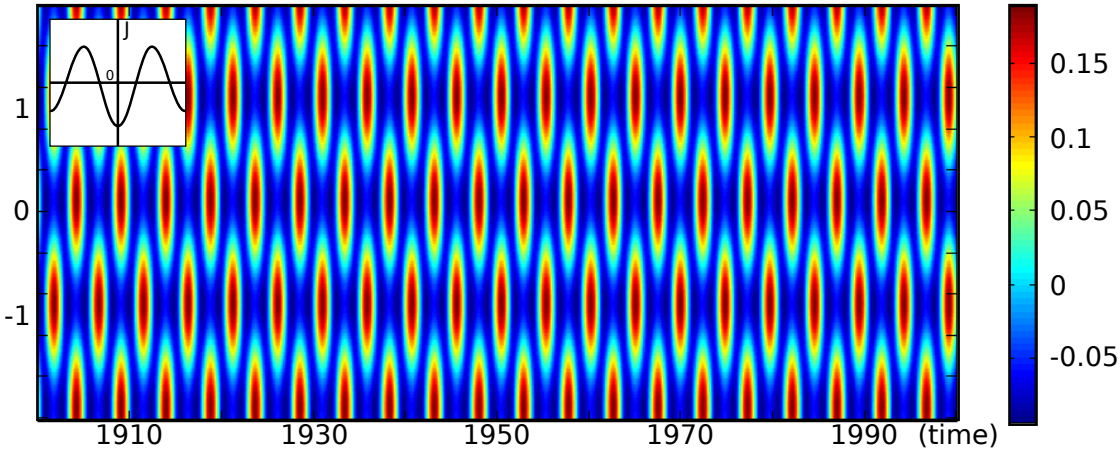


Figure 4: Stable solution of type (z_0, z_1, z_1) for the parameters $J = -\frac{2}{\pi}(0.2 \cos_2 + 0.9 \cos_4)$, $(c, D) = (1.5788, 0.6599)$, $h = 1$, $l = 0.99$, $\sigma_{s_1} = 3$. The bifurcation diagram was computed with proposition 4.2 and the stability of the solutions is based on the results in [CGK86]. Figure produced by numerical integration of (1) for 200 variables in space, a Runge-Kutta integrator of order 4 and a Hermite interpolation of order 4. See Appendix A for more details. The insert shows the plot of the connectivity function used in this example.

normal form, we can compute the stability of each solution type. It appears that in our numerical experiments, the Hopf bifurcation of the modulated solutions $(z_0, z_1, 0)$, (z_0, z_1, z_1) is difficult to exhibit. However the modulated solutions can easily be produced as shown in Figure 4.

The analysis in [CGK86] does not provide the phase diagram and we can find some partial answer by using the analysis of the Pitchfork-Hopf normal form. Indeed, if we use polar coordinates $z_k = \rho_k e^{i\theta_k}$, we find that the equations in ρ and θ are decoupled and we end up with a 3D real system of ordinary differential equations for the amplitudes ρ_i . Note that the equations for $(\rho_0, \rho_1, \rho_2 = 0)$ or (ρ_0, ρ_1, ρ_1) are the same type as (14) in the Pitchfork-Hopf bifurcation. We can then use [GH83] to find the phase diagram in the plane $z_2 = 0$.

5.7 Eight-dimensional case

The case of a Hopf-Hopf bifurcation between two non-zero Fourier modes is now partially investigated. Let us assume that we have the following eigenvectors:

$$\phi_1 = e^{i\omega_p\theta} e_p, \quad \phi_2 = e^{i\omega_p\theta} e_{-p}, \quad \phi_3 = e^{i\omega_q\theta} e_q, \quad \phi_4 = e^{i\omega_q\theta} e_{-q}$$

We use the coordinates $v_0 = z_1\phi_1 + z_2\phi_2 + z_3\phi_3 + z_4\phi_4 + c.c..$ The normal form has been studied in [CGK86] under the non resonance assumption, where it is shown that thirteen different types of solutions can be produced. However, if we consider the normal form truncated at cubic order as we do here for simplicity, only the stability of some particular types of solutions can be computed. These solution types are listed in the following table 1 where only the last four are new compared

type	solution	name
[1]	$(z_1, 0, 0, 0)$	Travelling wave
[2]	$(z_1, z_1, 0, 0)$	Standing wave
[3]	$(0, 0, z_3, z_3)$	Standing wave
[4]	$(0, 0, z_3, 0)$	Travelling wave
[7]	$(0, z_2, 0, z_4)$	Mixed-mode
[8]	$(0, z_2, z_3, 0)$	Mixed-mode
[12]	$(z_1, z_2, 0, z_4)$	Mixed-mode
[13]	$(0, z_2, z_3, z_4)$	Mixed-mode

Table 1: Table of solution types considered here.

to the previous bifurcations that we have studied. The stability conditions of these solutions are given in [CGK86]. Finally, we give the normal form truncated at the third order. Note that half of the coefficients are the same as for the $O(2)$ -Hopf normal form and the other half are computed in lemma I.1.

$$\begin{cases} \dot{z}_1 = z_1 \left(i\omega_p + a_1 + b_p^{(H)} |z_1|^2 + c_p^{(H)} |z_2|^2 + d_{(1)}^{(HH)} |z_3|^2 + e_{(1)}^{(HH)} |z_4|^2 \right) \\ \dot{z}_2 = z_2 \left(i\omega_p + a_1 + b_p^{(H)} |z_2|^2 + c_p^{(H)} |z_1|^2 + d_{(1)}^{(HH)} |z_4|^2 + e_{(1)}^{(HH)} |z_3|^2 \right) \\ \dot{z}_3 = z_3 \left(i\omega_q + a_3 + b_{(3)}^{(HH)} |z_1|^2 + c_{(3)}^{(HH)} |z_2|^2 + b_q^{(H)} |z_3|^2 + c_q^{(H)} |z_4|^2 \right) \\ \dot{z}_4 = z_4 \left(i\omega_q + a_3 + b_{(3)}^{(HH)} |z_2|^2 + c_{(3)}^{(HH)} |z_1|^2 + b_q^{(H)} |z_4|^2 + c_q^{(H)} |z_3|^2 \right) \end{cases} \quad (17)$$

The expression of the coefficients a_k s is not given because it is very similar to the case of the six-dimensional Hopf-Hopf normal form.

6 Application to two types of connectivity functions

In this section, we present the bifurcation diagrams of (1) around the stationary solution $V = 0$ in the plane (c, D) . Then, we discuss the nonlinear dynamics around the bifurcation points that appear in the diagrams. We first study the *Mexican-hat* connectivity which favors stationary activity: this connectivity has been mainly used as a functional connectivity in some feature domain (see [BYBOS95, BBC00, BCG⁺01]). It has locally excitatory connections and laterally inhibitory connections. This connectivity is often used to produce stationary solutions through a static bifurcation.

Then, we study a connectivity function which is laterally excitatory and locally inhibitory, the so-called *inverted Mexican-hat* (see [VCM07, Hut08]). This connectivity is motivated by the

fact (stereotyped) that inhibition is localized and long-range connections are mainly excitatory in the mammal visual cortex (see [LAB03]). By construction, this type of connectivity favors the spread of activity.

In both cases, we study spatially extended connectivities given by two spatial Fourier modes. To describe more localized connectivities requires more Fourier modes, and in this case we expect an increase in the number of bifurcations.

6.1 Mexican-hat connectivity

We write the connectivity $J(x) = (J_0 + J_1 \cos(2x)) \frac{2}{\pi}$ with $J_0 = -1$ and $J_1 > 1$ in order to generate locally excitatory connections. It follows that there is a Pitchfork line $\sigma_P = \frac{l}{s_1 J_1}$ which is shown in the bifurcation diagram in Figure 5 left labelled as (P). Two time-evolutions are also shown in Figure 5 Right in the neighborhood of the Pitchfork bifurcation. The x-axis of the

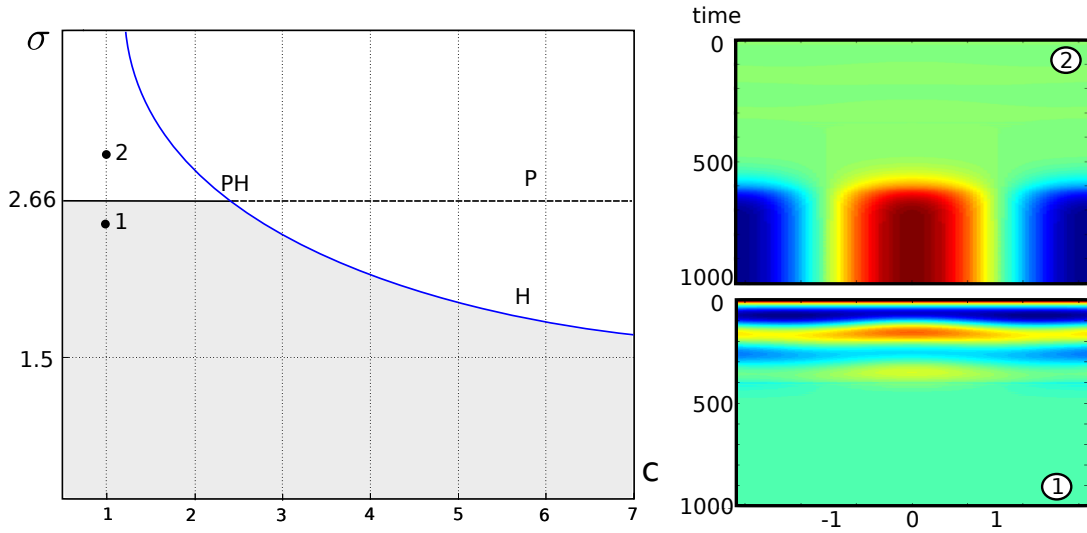


Figure 5: Left : bifurcation diagram in the plane (c, σ) , P is the Pitchfork line, H is the Hopf curve. Right : Time evolution corresponding to the points labelled 1 and 2 in the bifurcation diagram on the left. The grey region where the solution $V = 0$ is stable. We used $J_1 = 1.5$, $l = 1$.

bifurcation diagram in Figure 5 left is c : we will see that the diagram stays qualitatively the same if we use the constant delays D instead. We want to look at the possible intersection of the Pitchfork line with a Hopf curve.

6.1.1 Constant delays

Let us first consider the case of constant delays $c = 0$. We know from proposition 4.1 that there is only one Hopf curve (for the Fourier mode $n = 0$) in the plane (σ, D) , its analytical expression was also given. Recall that a necessary and sufficient condition for the existence of a critical delay D_0 is $2s_1\sigma J_0 \leq -l$ i.e. $\sigma > \frac{l}{2s_1}$: the Hopf curve intersects the Pitchfork curve at the Pitchfork-Hopf bifurcation point if $2\frac{|J_0|}{J_1} > 1$. This Hopf bifurcation cannot generate travelling waves or standing waves because it happens in the 0-mode. This is also true at the Pitchfork-Hopf bifurcation point as we will see below.

The phase diagram is characterized in [GH83]. We are particularly interested in the appearance of the quasi-periodic solution described in Section 5.4 because it is a striking behavior compared to the dynamics produced by the Hopf bifurcation. Recall that this solution produces a quasi-periodic solution and its existence depends on the conditions $\Delta > 0, b_n^{(P)} \Re(b_0^{(H)}) < 0$. We plot the sign of Δ as function of (J_1, h) where h is the threshold, in Figure 6 left, we also found that $b_1 \Re(c_2) > 0$ for all parameters $h, J_1 \in [0, 2]$ and this indicates that the doubly periodic solution does not exist in our network because $J_1 > 1$.

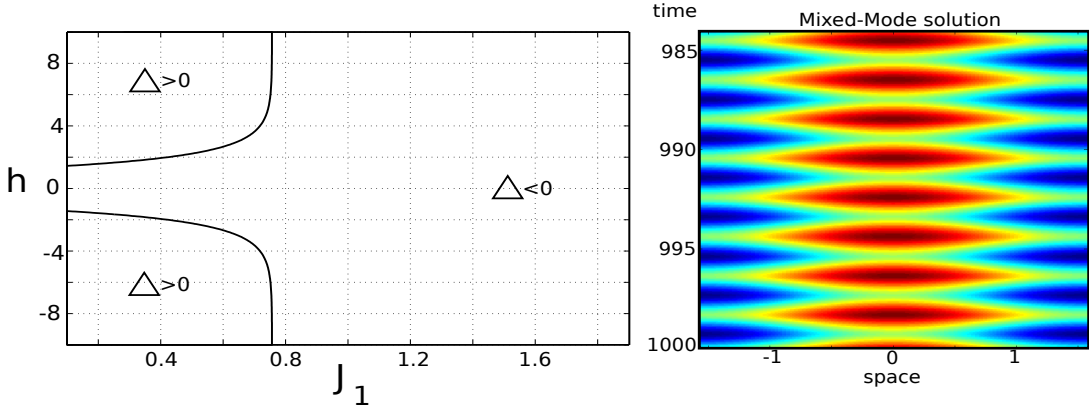


Figure 6: Left: Sign of Δ as a function of (J_1, h) . Green means positive. Right: example of a (unstable) Mixed-Mode solution for $J_1 = 1.5, h = 1, \sigma - \sigma_{PH} \approx 0.0127, D - D_{PH} \approx -0.0027$. The number of space variables in the discretization of (1) is $N = 200$.

The interesting solution, which does not appear in the other bifurcations discussed so far, is the Mixed-Mode solution (associated to the point O_{PH} in Section 5.4). This solution is a superposition of the static bifurcated state and the oscillatory solution: $V(x, t) = v_1 \cos(2x) + v_2 \cos(\omega_{PH}t)$, for some v_1, v_2 . The Mixed-Mode solution exists when $\Delta \neq 0$. More precisely, we find that in the region where $\Delta > 0$ (resp. $\Delta < 0$), the system has the phase diagram Ia (resp. Ib) in [GH83], modulo a time reversal.

For $J_1 > 1$, *i.e.* in the Mexican-hat case, the solution is found to be unstable. Thanks to the computation of the normal form, it is straightforward to select parameters and put the system very close to the Mixed-Mode solution before it decays to $V = 0$, see Figure 6 Right.

The other interesting feature of the phase diagram for $J_1 > 1$ is the bi-stability between the stationary solution $v_1 \cos(2x)$ and the oscillating solution $v_2 \cos(\omega_{PH}t)$, which are both stable for particular values of the couple (σ, D) , as shown in Figure 3 Red. The cortical state V can switch from a stationary state to an oscillatory state (and vice-versa) upon application of the correct external stimulation I_{ext} .

To sum up, the bifurcation portrait is composed of a Pitchfork line, a Hopf curve in the 0-mode and a Pitchfork-Hopf point. The phase diagram is the same for all $J_1 > 1, -2 \leq h \leq 2$, as shown in Figure 3.

6.1.2 Space dependent delays

We now consider the case of propagation delays. We want to know if the previous instabilities remain and what are the critical values of the constant delays/propagation delays. Using the

⁵This phase diagram is not shown because it does not appear in our model for which $J_1 > 1$.

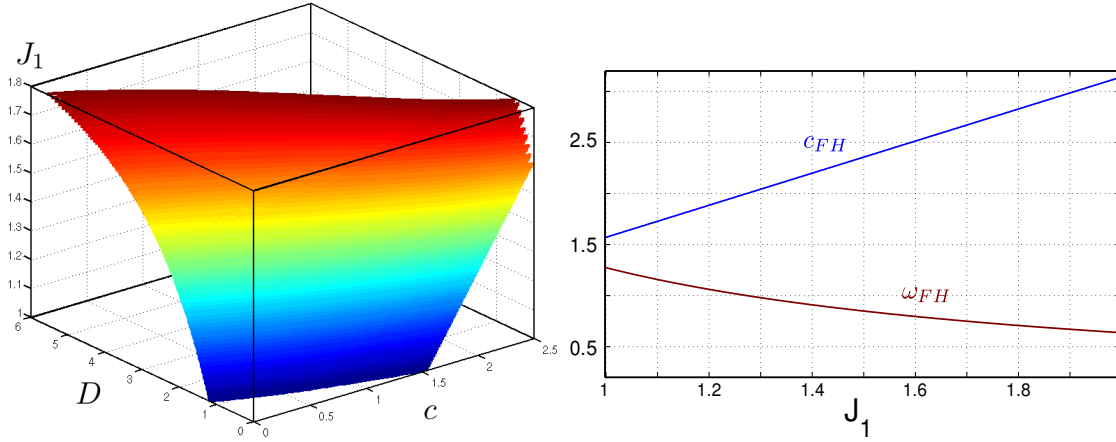


Figure 7: Left: Pitchfork-Hopf bifurcation surface in the parameter space (c, D, J_1) . Right: plot of c_{PH} (blue) and ω_{PH} (red) as function of J_1 where $D = 0$, *i.e.* the case of purely propagation delays.

proposition 4.2, we compute the Hopf curves in the parameter plane (D, c) for each Fourier coefficient J_1 (not shown). It appears that for $c \leq 10$, only the Hopf curve in the 0-mode appears, which is very similar to the case of purely constant delays, *i.e.* $c = 0$. We also find that the Hopf curve and the Pitchfork line intersect in a Pitchfork-Hopf bifurcation point for all $J_1 \in [1, 2]$. Hence we have computed the Pitchfork-Hopf surface in the space (c, D, J_1) , see Figure 7 left. Using the normal form given in Section 5.4, we can compute the phase diagram of the Pitchfork-Hopf bifurcation point in the space (c, D, J_1) for different thresholds $h \in [-2, 2]$. We find that it is the same as for constant delays, *i.e.* *Ib* (see Figure 3). Hence compared with the constant delay case, no new behavior appears.

To conclude, for the *Mexican-hat* connectivity considered in this section, the bifurcation diagram is quite simple: there is a Pitchfork line and a Hopf curve in the mode $n = 0$. When these two curves intersect at a Pitchfork-Hopf point, it produces one phase diagram that we completely characterized (see Figure 3). In particular, we found numerically that the quasi-periodic solution cannot occur and that bi-stability between an oscillatory solution and a stationary solution exists in a limited region of the parameter space.

6.2 Inverted Mexican-hat connectivity

We study a particular connectivity function $J(x) = -(0.5 + J_1 \cos_2) \frac{2}{\pi}$ and $J_1 > 0.5$. Unless otherwise stated, we chose $J_1 = 2.1$ in order to have local inhibition and lateral excitation (see Figure 8). Let us first note, that because the two Fourier modes of the connectivity are negative, no static bifurcation can occur; this is not generally true for *inverted Mexican-hat* connectivities because, for localized connectivities, more Fourier modes are non-zero and some are possibly positive. In our case, we can nevertheless restrict ourselves to searching for oscillatory behaviors. We start with constant delays and then extend the analysis to include space dependent delays.

6.2.1 Constant delays

According to proposition 4.1, an equivariant Hopf bifurcation happens for some constant delay D_n in the Fourier mode n if the connectivity has negative eigenmodes. Using the same proposition,

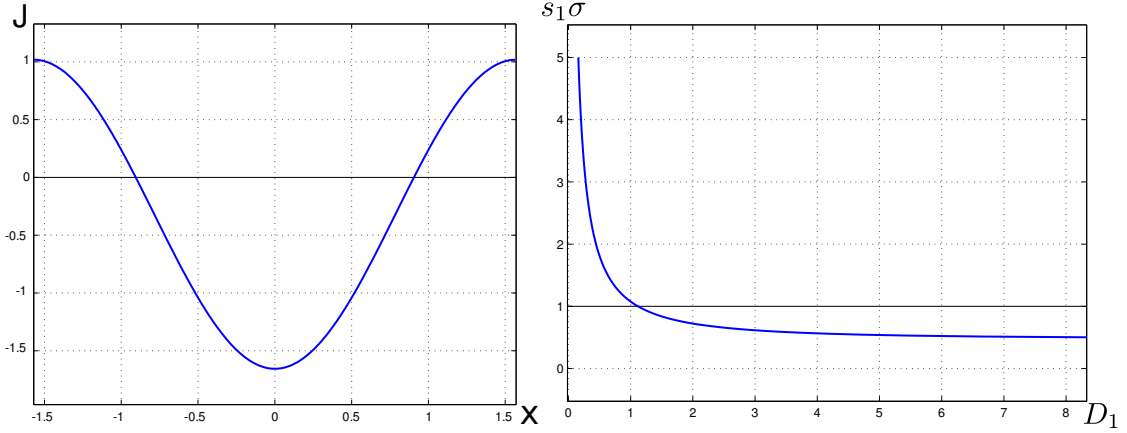


Figure 8: Left: connectivity used in the examples of this section ($J_1 = 2.1$). Right: plot of the critical constant delay D_1 (for the mode $n = 1$) as function of the nonlinear gain σ .

we find that it is the mode $n = 1$ that first bifurcates for $c = 0$ when varying D . We plot the constant critical delay D_1 as function of the nonlinear gain σ in Figure 8 Right: if the nonlinear gain σ is small, *i.e.* if the network is linear, then it is not possible to generate oscillations because $D_1 \rightarrow \infty$ as $s_1 \sigma J_1 \rightarrow 1$. The fact that the Hopf produces stable travelling waves was also proven⁶

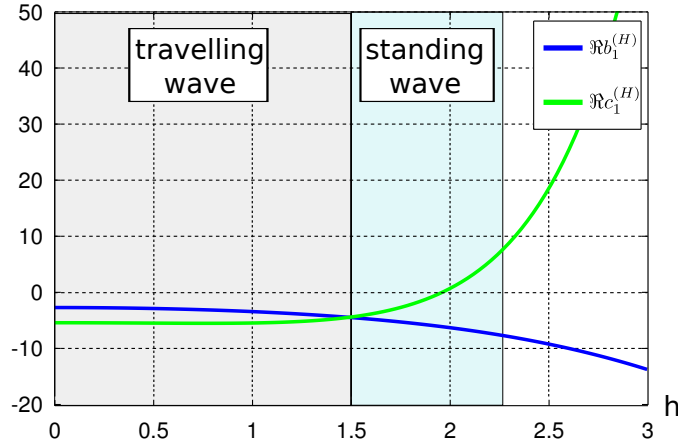


Figure 9: Plot of the real part of the $O(2)$ -Hopf normal form coefficients as function of the threshold h for $s_1 \sigma = 1$, $c = 0$, $D = 1.119$, $J_1 = 2.1$, $n = 1$. The stability of the travelling waves and the standing waves is shown.

in [RM11]. However, when looking at the dependence of the coefficients of the $O(2)$ -Hopf normal form as function of the threshold h , we see on Figure 9 that the stability of the wave can change. At small contrasts, the travelling waves are stable. Then, the standing waves become stable and at large thresholds $h > 2.25$, there are only unstable travelling waves. An example of such waves is given in Figure 10

⁶for a different varying parameter.

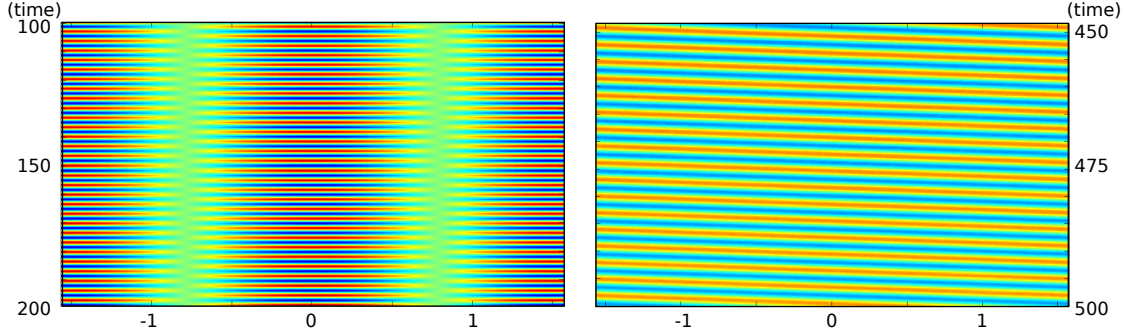


Figure 10: Plot of the different stable solutions at a $O(2)$ -Hopf bifurcation point. Left: standing wave, $h = 2$. Right: travelling wave, $h = 0$. The space discretization of (1) is $N = 300$. Parameters: $s_1\sigma = 1$, $c = 0$, $D = 1.119$, $J_1 = 2.1$.

6.2.2 Space dependent delays

We now study the case of space dependent delays *i.e.* $c > 0$. In this case, we expect changes in the bifurcation diagram. We know from [VF11] that if the nonlinear gain σ is too small, oscillations are impossible. Hence, we expect a strong dependency of the Hopf curves on the nonlinear gain. This is shown in Figures 11 and 12 where $s_1\sigma = 0.5$ in the left panel and $s_1\sigma = 1$ in the right panel. There are three interesting features that come out of these figures:

1. No Hopf curve crosses the c -axis for $s_1\sigma < 2$: it is impossible to produce oscillations with only propagation delays in this case. This is shown up to $s_1\sigma < 1.3$, but further numerical investigations have led to this conclusion (data not shown). For $s_1\sigma > 2$, the Hopf curve for the 0-mode crosses the c -axis, more Hopf curves do this as σ is increased. We could not find a criterion to predict when a Hopf curve crosses the c -axis.
2. The accumulation of the Hopf curves around $c \approx 10$ (see Figure 12 left): for small changes in the constant delays, a lot of eigenvalues cross the imaginary axis. Very sophisticated dynamics should happen in this parameter region.
3. The number of intersections between Hopf curves, shown with black dots (in particular in Figure 12 left). These intersection points are Hopf-Hopf bifurcation points where the dynamics can lead to complicated behaviors (see [GH83, CGK86, Kuz98]).

Let us go back to Figure 11 where we have plotted the Hopf curves for $s_1\sigma = 1$; the grey part is the parameter region where the stationary solution $V^f = 0$ is asymptotically stable. For small propagation delays $c \approx 0$, by increasing the constant delay D , it is the 1-mode that first bifurcates and we find solutions like those shown in Figure 10. For larger values of c , it is the 0-mode that first bifurcates, hence giving a non-equivariant Hopf bifurcation. Thus, we find the rather surprising fact that even if the connectivity does not have a sufficiently negative eigenmode (*i.e.* $s_1\sigma J_0 = -1$), Hopf bifurcations may still appear due to the intricate interaction between the connectivity and the propagation delay functions. Hopf bifurcations can also happen in modes that are not present in the connectivity as shown in Figure 12: for example there is a Hopf curve in the 2-mode whereas the connectivity has no 2-mode. We have not been able to find a simple criterion to predict the appearance of an oscillatory solution as we did for constant delays in Section 4.1.

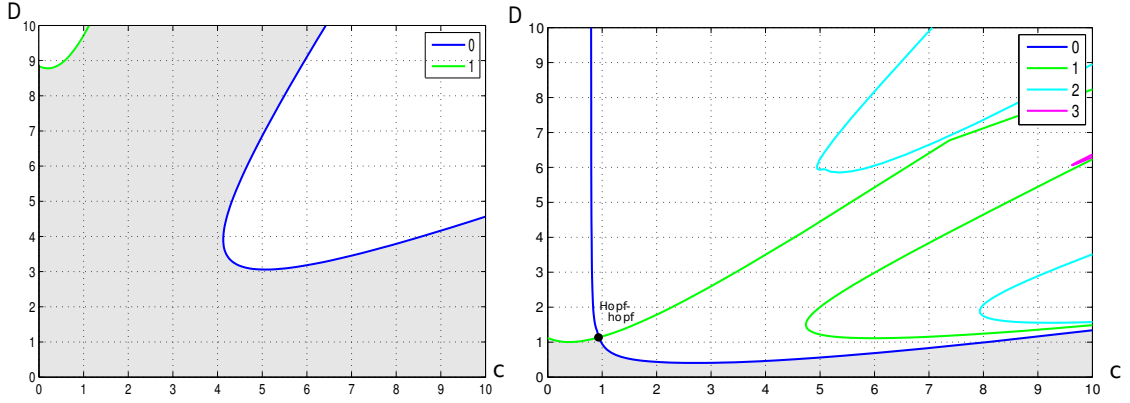


Figure 11: Plot of the Hopf curves in the (c, D) plane for $s_1\sigma = 0.5$ (left) and $s_1\sigma = 1$ (right). The different Hopf curves are labelled with the corresponding Fourier mode. The grey part is where the stationary state $V^f = 0$ is asymptotically stable.

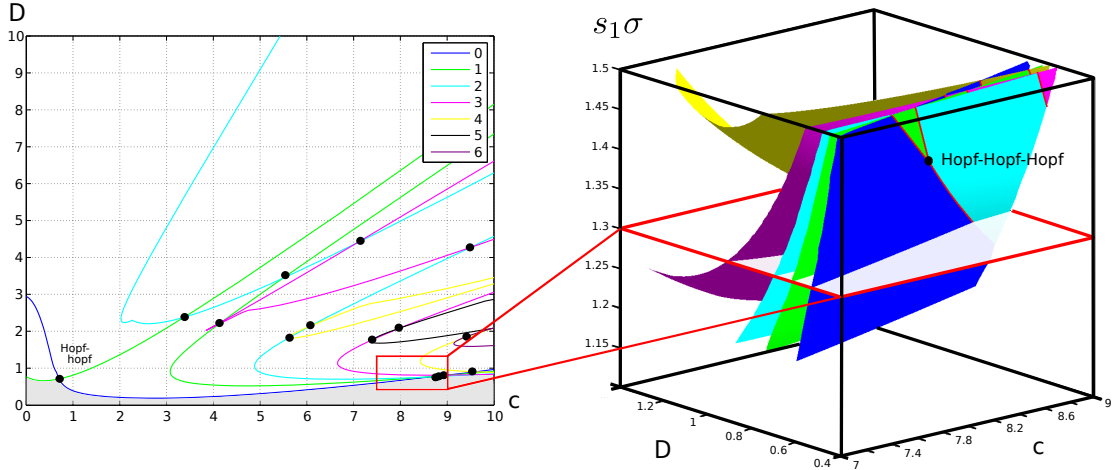


Figure 12: Left: plot of the Hopf curves in the (c, D) plane for $s_1\sigma = 1.3$. Right: plot of the Hopf surfaces in the (c, D, σ) space for a particular region which is shown in the 2D bifurcation plot. The Hopf-Hopf curves, intersection of two Hopf surfaces are shown in red. Finally, two Hopf-Hopf curves intersect at a Hopf-Hopf-Hopf bifurcation point.

Remark 3 Finally, for $(c, D, s_1\sigma) \approx (8.0584, 0.6023, 1.412)$, we find an intersection between three Hopf curves in the Fourier modes 0, 1, 2. It is difficult to see this interaction in the 2D bifurcation planes. This is why we show in Figure 12 Right a selected region of the 3D parameter space (c, D, σ) with the plot of the Hopf surfaces given by proposition 4.2. This intersection is a codimension three Hopf-Hopf-Hopf bifurcation point which we have not studied.

6.2.3 Six dimensional Hopf-Hopf bifurcations

Let us say a few words about the Hopf-Hopf bifurcation points: based on the normal form study in Section 5.5, we have looked at the Hopf-Hopf bifurcation point between the 0-mode and the

1-mode under the non-resonant assumption $\frac{\omega_0}{\omega_1} \notin \mathbb{Q}$.

We follow numerically (see Section A) in the two parameters $(J_1, s_1\sigma) \in [0.5, 3] \times [0, 3]$ the two Hopf-Hopf bifurcation points in the mode interaction $0 : 1$. These are the most 'stable' six-dimensional Hopf-Hopf bifurcations and there are two of them: close to $c = 0$ or close to $c = 10$. Then, for each bifurcation point for a particular value of $(J_1, s_1\sigma, c, D)$, we compute the stability of the possible solutions as function of (h, l, σ) based on the formulas in [CGK86]. We find bistability between the solutions $(z_0, 0, 0)$ and $(0, z_1, 0)$ (or $(0, z_1, z_1)$). The mixed-mode solution $(z_0, z_1, 0)$ is never stable while the mixed-mode solution (z_0, z_1, z_1) is stable at high thresholds $h \approx 2.5$ but the stability region is so tiny in the plane (σ, l) that they never show up in the numerical simulations.

Hence, the dynamics are simple in this case and are composed of travelling or standing waves in the spatial Fourier mode 0 or 1: the stability of these solutions is dependent on the threshold h as we have seen in the case of the Hopf bifurcation (see Figure 9). High thresholds favor standing waves and small thresholds favor travelling waves.

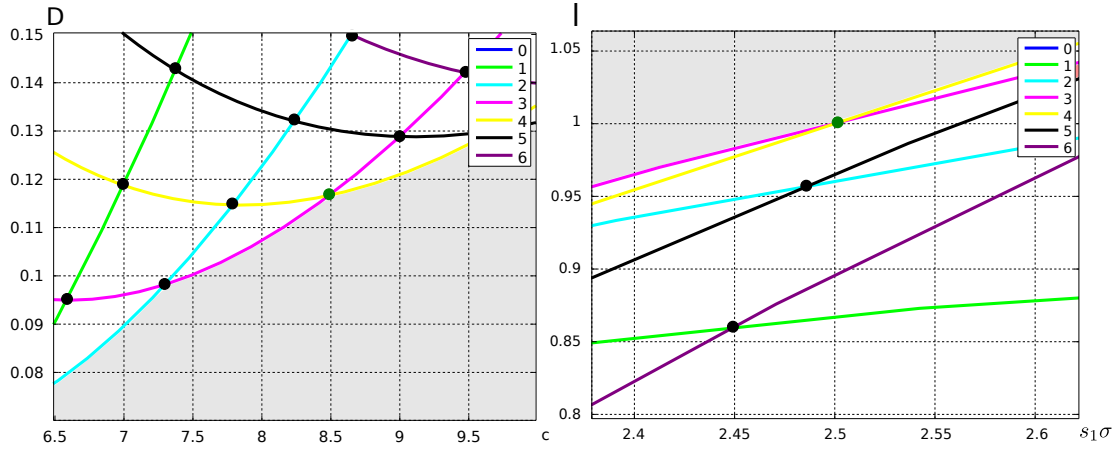


Figure 13: Left: plot of the Hopf curves in the plane (c, D) for $s_1\sigma = 2.5$. Right: plot of the Hopf curves in the plane $(s_1\sigma, l)$ for $(c, D) = (8.4873, 0.1167)$, based on the formula given in corollary 4.3. The Hopf-Hopf bifurcation are marked with a black dot. The green dot marks a particular Hopf-Hopf bifurcation that is studied in the text. The grey region represent the stability region of the point $V = 0$.

6.2.4 Eight dimensional Hopf-Hopf bifurcations

In the case of the eight-dimensional Hopf-Hopf bifurcations (at least for the most 'stable' ones) we did not follow the same approach of performing numerical continuation of every bifurcation point and computing their phase diagram. Indeed, as can be seen on Figure 12 or Figure 13 left, the bifurcation points accumulate and the higher the nonlinear gain σ , the more bifurcation points there are. It is then very time-consuming to follow them all and perform the same analysis as we did for the six-dimensional Hopf-Hopf bifurcation points.

We computed the bifurcation diagrams for some nonlinear gains $s_1\sigma \in \{1.3, 2, 2.5\}$ and the interactions $1 : 2$, $2 : 3$, $3 : 4$ and $4 : 5$ near the stability border for the state $V = 0$ (shaded in grey in Figure 13). In all cases, we checked that the ratio of the frequencies ω_p/ω_q can not be approximated by a fraction $\frac{r}{s}$ at 1% with $r + s < 5$, hence giving weak resonances. We found that only the interaction $3 : 4$ can produce stable mixed-mode solution of type [8] (see table 1).

All these bifurcations produce bistability between the travelling waves and the standing waves (see the stability diagram in Figure 14 of the Hopf-Hopf bifurcation marked with a green dot). Figure 14 shows the stability regions of each solution type in table 1 as function of the threshold h for the 3 : 4 interaction. We note the multistability of the travelling (resp. standing) wave solutions for the different values of the threshold h . In particular, the standing wave solutions are stable for thresholds $1.2 < h < 2.2$: this is similar to what we found for the $O(2)$ -Hopf bifurcation in Figure 9.

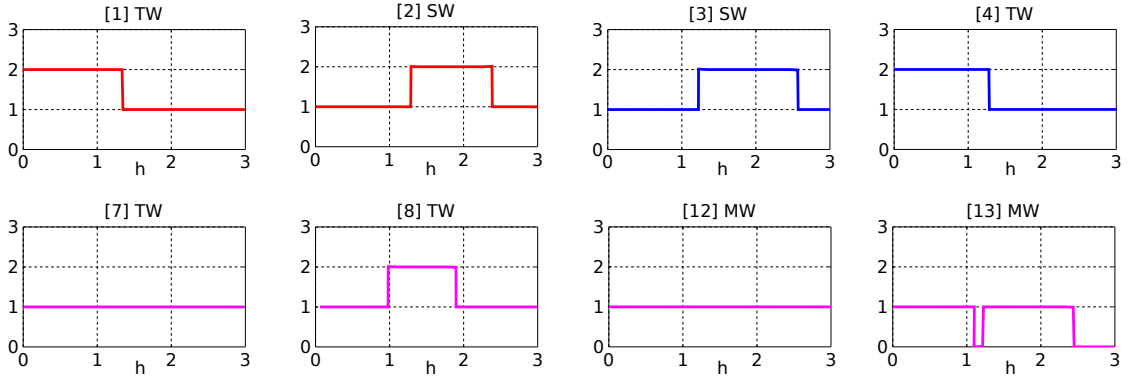


Figure 14: Stability diagram in the parameter plane (σ, l) of the solutions in table 1 as function of the threshold h . The code is the following: 0 codes for non-existence, 1 codes for unstable solution and 2 codes for a stable solution. The Hopf-Hopf bifurcation considered here is the one marked with a green dot in Figure 13. It occurs for $(c, D) = (8.4873, 0.1167)$ and $s_1\sigma = 2.5$. SW = Standing Wave, TW = travelling wave, MW = Modulated wave.

The stability diagram in Figure 14 also shows that the solution [8] is stable for an extended region of the parameter space. However, Figure 14 does not give the eigenvalues⁷ of the Jacobian at the solution [8] which are in fact much smaller, although negative, than the ones of the solutions [1], [2], [3], [4]. Hence to reach this precision at which [8] is stable requires a very large numerical discretization of (1). Practically, given the size of the eigenvalues at the solution [8], we are not sure that the solution [8] shown in Figure 15 is stable although its amplitude does not vary on long time scales.

One could argue that by using larger values of l, σ , we could have larger eigenvalues and thus the simulation of (1) near the solution [8] would be easier. However, as we shall explain now, we are forced to be very close to the bifurcation point for the normal form in lemma I.1 to be valid numerically. Indeed, it appears that the bifurcations are very close in the plane $(s_1\sigma, l)$ when (c, D) is set at the value $(8.4873, 0.1167)$ of the 3 : 4 Hopf-Hopf bifurcation (marked with a green dot in Figure 13). Figure 13 Right is interesting in that it tells us how far can we go from the Hopf-Hopf bifurcation point without crossing another bifurcation. The range is quite narrow in l as we find roughly the following upper bounds $|\delta l| < 0.05$ and $s_1|\tilde{\sigma}| < 0.05$. This range limits the value of the eigenvalues of the solution type [8] and thus its simulation. This also shows that the predictive power of the Hopf-Hopf normal forms is numerically limited here because the Hopf-Hopf bifurcation points are very close to each other. Hence, the phase space would be better understood if one could study the interaction of two Hopf-Hopf bifurcation points (*i.e.* with a sixteen-dimensional space). This seems very difficult theoretically given that the Hopf-Hopf bifurcation is not entirely understood yet (see [CGK86]).

⁷Note that these eigenvalues are computed using the normal form coefficients given in lemma I.1 and the integrals appearing in the expression of these coefficients are computed numerically with high precision.

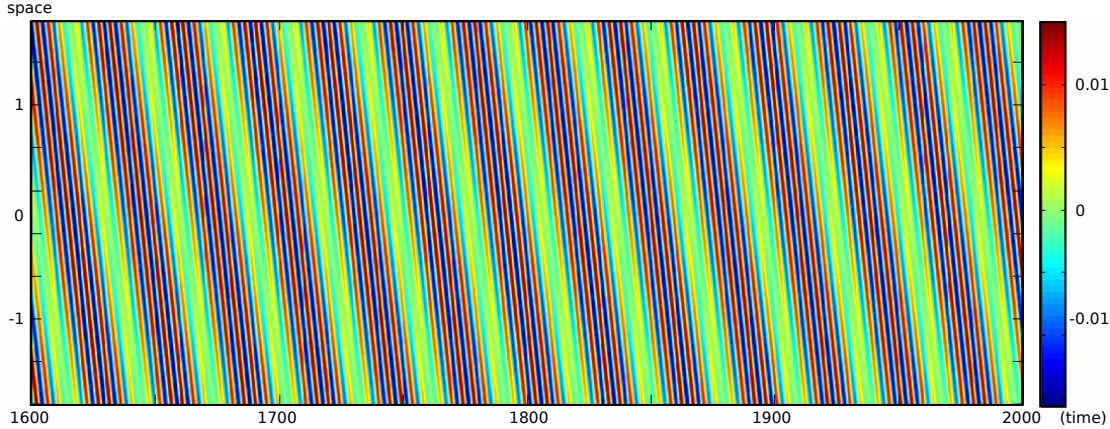


Figure 15: Plot of a stable mixed-mode solution of type [8] (see table 1) at the Hopf-Hopf bifurcation 3 : 4 marked with a green dot in Figure 13. The parameters are $(c, D) = (8.4873, 0.1167)$, $s_1\sigma = 2.51$, $h = 1.75$, $l = 0.99$. The discretization is $N = 901$ unknowns in space. The frequencies of the two Hopf bifurcations are $\omega_p = 1.2799$, $\omega_m = 1.4940$.

6.2.5 Symmetry breaking effects

We wish to give a simple numerical example of what can happen when the system is put far from the 3:4 Hopf-Hopf bifurcation point. We find similar results near the interaction 2 : 3 which suggests that the following phenomena are robust. In Figure 16, we chose the parameters $l = 0.9$, $s_1\sigma = 2.53$ so that the system is past the 2 : 5 Hopf-Hopf bifurcation (see Figure 13 Right). We find what seems⁸ to be a periodic orbit where a travelling wave in the mode 2 periodically appears (see Figure 16 Bottom Right). The transient between the appearances of the travelling wave is shown in Figure 16 Bottom Left. The period of the solution is very long as can be seen in Figure 16 Top which shows the modulation of the coefficient of the first Fourier cosine modes \cos_n .

Note that this result is a bit surprising given that we expect the 2 : 5 Hopf-Hopf bifurcation to be in the unstable manifold of the equilibrium $V = 0$. Only the numerical continuation of the bifurcated solutions from the 3 : 4 Hopf-Hopf bifurcation would allow to precisely study the existence of secondary bifurcations. Indeed, the periodic solution in Figure 16 occurs for a threshold around $h \approx 0.5$ and we have not detected changes in the stability diagrams of the 3 : 4 Hopf-Hopf bifurcation (see Figure 14) and the 2 : 5 Hopf-Hopf bifurcation (data not shown) around the threshold value $h = 0.5$. Another explanation for the appearance of the periodic solution comes from the symmetry breaking of the translation equivariance by our numerical scheme (see more details in Section A). Indeed, it is known that the perturbation of equivariant systems can dramatically change the phase diagram (see [CL00] and [DK91] for the symmetry breaking of the $O(2)$ -Hopf bifurcation) by creating periodic solutions or heteroclinic cycles, for example.

⁸Figure 16 only shows a snapshot of an evolution computed for $t < 6e4$.

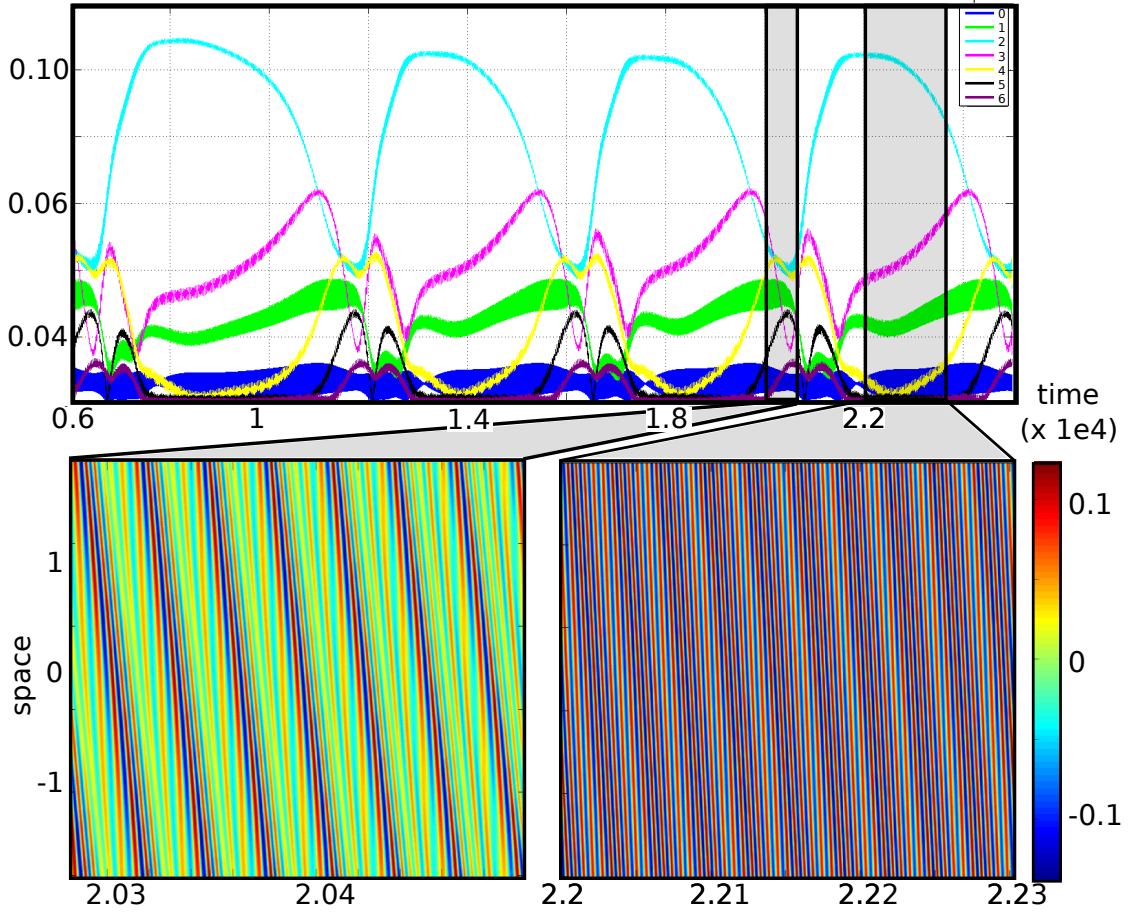


Figure 16: We write $V(x, t) = V_0(t) + \sum_{p=0}^{\infty} V_p^{(c)}(t) \cos_p(x) + V_p^{(s)}(t) \sin_p(x)$. Top: plot of the functions $t \rightarrow \mathcal{H}(V_p^{(c)}(t))$ where \mathcal{H} is the Hilbert transform. Bottom: zoom in on a specific part of the time evolution Parameters $h = 0.5$.

7 Discussion and conclusion

In this work, we have applied the tools developed in [VF12] to a scalar neural fields model with homogeneous connectivity, space-dependent delays and periodic boundary conditions. The motivation stems from the lack of studies concerning the interplay between constant delays and propagation delays. We found very rich bifurcation diagrams despite the simplicity of the model studied here.

Based on the analytical formula of the Hopf bifurcation curves given in [Vel11], we were able to compute the normal form of the main bifurcations that appear in the bifurcation diagrams. Compared to the weakly nonlinear method (see [VCM07, BK08, RBH05, RM11]), the normal form theory has the advantage of providing the theoretical background to ensure that the reduced equations are a good approximation of the dynamics. Despite this fact, we did not find any differences in the expression of the coefficients of our normal forms with the one given in [VCM07,

[RM11](#)].

A first difficulty is related to an apparent paradox: despite having an analytical formula for the Hopf bifurcation curves, we could not find a criterion to predict the global layout of the Hopf bifurcation curves in the case $c > 0$. In the case $c = 0$, we found a very simple condition for the existence of the Hopf curves. Hence, the connectivity function strongly affects the layout of the Hopf bifurcation curves and this is why it is difficult to predict how delays influence the dynamics.

We have studied two simple connectivity functions (with two spatial Fourier modes) based on the computation of the coefficients of the main normal forms. The first case is that of the Mexican-hat connectivity which has been frequently used to describe spontaneous stationary activity. We found that adding delays only introduces a Hopf bifurcation curve in the mode 0 in the bifurcation diagram. The interaction of this Hopf bifurcation with the static bifurcation gives a Pitchfork-Hopf bifurcation which has been completely characterized: in particular there is no mixed-mode solution. We also found bistability between non trivial stationary activity and uniformly oscillating activity in some parameter region. We believe that the study of more localized connectivity would produce a steady-state/Hopf interaction in two nontrivial spatial Fourier modes which can give complicated dynamics.

We have looked at the inverted Mexican-hat connectivity and we find very interesting bifurcation diagrams with numerous Hopf/Hopf interactions. We have shown that the $O(2)$ -Hopf bifurcation can produce stable standing waves if the threshold is nonzero ; this is different from the results reported in [\[RBH05, VCM07, RM11\]](#). Then, we have looked at the six-dimensional Hopf-Hopf bifurcations and we have not found any stable mixed-mode solution. However, as shown in Figure 4, moderate changes in the connectivity function can alter this conclusion as the mixed-mode solutions are stable in this case. Finally, we find bistability between travelling (resp. standing) waves and the uniformly oscillating solution. We also looked at the eight-dimensional Hopf-Hopf bifurcations for which the mixed-mode solutions are stable in some cases. However, their attracting set is much smaller than the set of the traditional waves. Also, the fact that the Hopf-Hopf bifurcations accumulate makes the mixed mode solution difficult to observe. Again, this conclusion is strongly dependent on the connectivity function.

Finally, we have shown numerical simulations of evolutions far from the main bifurcations in the region where the Hopf bifurcation curves accumulate. We found periodic solutions whose period is composed both of a transient and a travelling wave. Further studies are required in order to know if these solutions come from secondary bifurcations or from the symmetry breaking of the translation invariance by our numerical scheme. This will be the subject of further studies.

A limited number of papers [\[VCM07, RM11\]](#) has looked at the quantitative effects of the delays on the nonlinear dynamics of neural fields networks. Most of the literature is devoted to the linear stability analysis and on bounds for the stationary solution to remain stable after the introduction of delays. To the best of our knowledge, this work is the first study concerning the interplay between constant delays and space-dependent delays at a quantitative level. Compared to the case of constant delays, there is a coupling between the connectivity function and the space dependent delays. Hence, oscillations can appear in Fourier spatial modes that are not present in the connectivity function. This is why moderate changes in the connectivity pattern can strongly affect the dynamics.

This work suggests for several extensions. The first is to look at the nonlocal dynamics and study secondary bifurcations in order to better understand what happens in the region where the Hopf curves accumulate. We have not looked at the case of a distribution of speeds (see [\[AH06, BL10\]](#)) for the space dependent delays. This would be an analysis very similar to the present work with mainly quantitative differences. A very interesting extension would be to study neural fields with second order time dynamics. This seems more amenable than the case

of two populations. It would very likely yield to new dynamics. We cannot predict at this stage whether the mixed mode solutions and other aperiodic solutions will appear in this case. A very exciting study concerns the interaction between the spontaneous activity and the external input (which has been neglected in our work). In particular, if the neural fields are periodically forced, we expect sophisticated behaviors depending on the amplitude and the frequency of the forcing. An interesting aspect, not covered in this work, is the interaction between neuronal/synaptic adaptation and delays. This has largely been ignored in the literature (we are only aware of the work of Venkov and co-workers) despite the usefulness and applicability to visual cortex models. Indeed, if after some intense period of activity, a hypercolumn is required to rest for some time δt regardless of its afferent inputs, it can only “see” hypercolumns at distance $v\delta t$, where v is the propagation speed of signals along axons. It seems that interesting behaviors, for biology and pattern theory could emerge from this interaction. The analysis of such models could be done with our tools without much change. Finally, a promising study concerns the effect of multiplicative noise on neural fields models. In some cases [Tou12], the equations simplifies and the equations for the mean membrane potential and the variance of the membrane potential couple through generalized neural fields equations with spatio-temporal delays. The application of the methods of the present work to these equations could bring clue about the quantitative relationship between delays and noise.

Acknowledgement

The author would like to thank Hosam Yousif and Ben Regner for their valuable comments and criticisms on this manuscript.

A Numerical tools

In order to compute time evolutions which are solutions of the equation (1), we need to compute numerically the following integral while maintaining the reflection (resp. translation) symmetries. We first transform the integral:

$$\begin{aligned} \int_{-\pi/2}^{\pi/2} J(x-y)U(y, t - \tau(x-y))dy &= \int_{-\pi/2}^{\pi/2} J(z)U(x-z, t - \tau(z))dz \\ &= \int_0^{\pi/2} J(z) [U(x-z, t - \tau(z)) + U(x+z, t - \tau(z))] dy. \end{aligned}$$

The advantage of the last term is that it makes the reflection equivariance independent of J : no change of variable is needed. Then, we use the Trapeze or the Simpson method to compute the last integral numerically. When numerically tested with $\cos(2x - \lambda t)$, we find the L^2 -error for the reflection equivariance to be very close to zero *e.g.* $\sim 1e - 15$. However, the translation equivariance error is not that small although it decreases with the space discretization.

By discretizing the space, we end up with delay differential equations (DDE) with constant delays. We use the *C++* library `dde` to solve numerically these DDE and *openMP* to parallelize the for-loops. The library `dde` implements many algorithms and gives the choice between a Continuous interpolation or an interpolation with Hermite polynomials of order 4 for the values of the history segments. We find it difficult to make the evolution respect the symmetries: we

find that we need to round off the integral values at 10^{-9} . We tested the respect of equivariance by our numerical scheme by putting the system at a $O(2)$ -Hopf bifurcation where the standing wave is unstable (see Figure 2). Then, we find that our program, initially set on the subspace of standing wave solutions, remains on this subspace for very long evolutions.

Using numerical continuation techniques provided by the *C++* library Trilinos (see [SHD04] and the [website](#)), we made a program to follow the six-dimensional Hopf-Hopf bifurcation points in the two parameters $(J_1, s_1\sigma)$.

B Cauchy problem

In order to apply a normal form theory to (1), we have to rewrite this equation as a Cauchy problem with a sufficiently smooth nonlinear righthand side. This was done in [VF12] and we now sum up the main results. Let us consider the two spaces

$$\begin{cases} \mathcal{X}^{(q)} \equiv L^q \times L^q(-\tau_m, 0; L^q), \\ \mathcal{Y}^{(q)} \equiv \{u \in L^q \times W^{1,q}(-\tau_m, 0; L^q) \mid \pi_1 u = (\pi_2 u)(0)\} \end{cases} \quad (18)$$

where $L^q \equiv L^q\left(\left[-\frac{\pi}{2}, \frac{\pi}{2}\right], \mathbb{R}\right)$ with the norms

$$\begin{aligned} \|\phi\|_{L^q(-\tau_m, 0; L^q)} &= \left(\int_{-\tau_m}^0 \|\phi(\theta)\|_{L^q}^q d\theta \right)^{\frac{1}{q}} \\ \|\phi\|_{W^{1,q}(-\tau_m, 0; L^q)} &= \|\phi\|_{L^q(-\tau_m, 0; L^q)} + \left\| \frac{d}{d\theta} \phi \right\|_{L^q(-\tau_m, 0; L^q)}. \end{aligned} \quad (19)$$

and let us introduce the continuous linear operator $\mathbf{A} \in \mathcal{L}(\mathcal{Y}^{(q)}, \mathcal{X}^{(q)})$

$$\mathbf{A} \equiv \begin{bmatrix} -\text{Id} & s_1 L_1 \\ 0 & \frac{d}{d\theta} \end{bmatrix}. \quad (20)$$

We also denote by π_1, π_2 the projectors on each component of $\mathcal{X}^{(q)}$. Then, we rewrite (1) as

$$\begin{cases} \dot{u}(t) = \mathbf{A}u(t) + \mathbf{R}(u(t), \mu) \\ u(0) \in \mathcal{Y}^{(q)} \end{cases} \quad \text{with} \quad \mathbf{R}(u, \mu) = \begin{bmatrix} L_1(\mu) \tilde{S}_0(\pi_2(u)) \\ 0 \end{bmatrix}. \quad (21)$$

where the nonlinearity S_0 is written $S_0(x) = s_1 x + \tilde{S}_0(V)$ with $\tilde{S}_0(x) \stackrel{x \rightarrow 0}{\sim} O(x^2)$. As a consequence, $\dot{u} = \mathbf{A}u$ is the linearization of the Cauchy problem near $u = 0$. It was proven that $\mathbf{R}(\cdot, \mu) \in C^{q-1}(\mathcal{Y}^{(q)}, \mathcal{X}^{(q)})$. Hence, we chose the integer q large enough such that $u \rightarrow \mathbf{R}(u, \mu)$ is sufficiently smooth to compute normal forms. It is useful to note that the $\mathcal{X}^{(q+1)} \subset \mathcal{X}^{(q)}$ and $\mathcal{Y}^{(q+1)} \subset \mathcal{Y}^{(q)}$. Hence, in the study of (21), we perform the linear analysis (*i.e.* computation of the spectrum and the spectral projector) in the Hilbert space $\mathcal{X}^{(2)}$ and the nonlinear analysis in a subset $\mathcal{X}^{(q)}$. In particular, we find that all the eigenvectors can be written $\phi = \begin{bmatrix} U(x) \\ e^{\lambda\theta} U(x) \end{bmatrix}$

where λ is an eigenvalue of \mathbf{A} .

Suppose that for a particular value μ_c of the parameter μ , we find a nonzero center linear set \mathcal{X}_c spanned by the eigenvectors ϕ_i associated to the eigenvalues of zero real part. We further assume that there are no eigenvectors of positive real part. Note that \mathcal{X}_c is necessarily finite dimensional. Then we proved in [VF12] that there is a nonlinear function Ψ describing the center manifold correction (as function of the parameters μ) and a differential equation, called the *reduced equation*, defined on \mathcal{X}_c

$$\frac{du_c}{dt} = \mathbf{A}u_c + P_c \mathbf{R}(u_c + \Psi(u_c, \mu), \mu), \quad (22)$$

where P_c is the (spectral) projector on \mathcal{X}_c defined in (25). For an initial condition $u(0)$ of (21) sufficiently close to $u = 0$, there is an initial condition $u_c(0) \in \mathcal{X}_c$ such that $u(t) - u_c(t)$ converges exponentially fast to zero. More details and properties can be found in [VF12].

C Normal form computation

Among all the different reduced equations, some of them produce the same dynamics up to a change of variable. Normal form theory aims at finding a polynomial change of variable which “simplifies” the reduced equation by removing the maximum number of terms at every order of its Taylor expansion. Once simplified, the truncation⁹, at order k , of the Taylor expansion of the reduced equation is a polynomial vector field which is called the *normal form*. In most of the cases, the truncation of the Taylor expansion of the reduced equation do not change the dynamics. If the reduced equation satisfies some properties, such as its linear part has a one dimensional null space, for example, in addition to some non-degeneracy conditions, then the simplified polynomial vector field has always the same monomials. These conditions are listed in [GH83, GS84, GSS88, Kuz98, HI10] as well as the corresponding normal forms. Moreover, these references also contain the study of the dynamical system associated to the normal form. Hence, there are two steps in finding the normal form:

- compute the Taylor expansion of the reduced equation,
- recognize which conditions are satisfied by the reduced equation and use the tabulated formulas in [GH83, GS84, GSS88, Kuz98, HI10] to extract the full dynamics of the delayed neural field equations on the center manifold.

If the normal form is not tabulated, then we need to compute the change of variable. This is lengthy because we need to compute the center manifold correction Ψ and then the polynomial change of variable. In fact, we can find the normal form directly without computing the center manifold correction Ψ as explained in [HI10]. More specifically, from the Cauchy problem

$$\frac{du}{dt} = \mathbf{A}u + \mathbf{R}(u, \mu), \quad \mathbf{R}(0, \mu_c) = 0, \quad D_u \mathbf{R}(0, \mu_c) = 0$$

we have a reduced equation (22) for $u_c \in \mathcal{X}_c$ with the center manifold correction Ψ :

$$u = u_c + \Psi(u_c, \mu), \quad \Psi(u_c, \mu) \in \mathcal{Y} \cap \mathcal{X}_c, \quad \Psi(0, \mu_c) = 0, \quad D_u \Psi(0, \mu_c) = 0.$$

This reduced equation is

$$\frac{du_c}{dt} = \mathbf{A}u_c + P_c \mathbf{R}(u_c + \Psi(u_c, \mu), \mu).$$

Then, we apply a change of variable to u_c

$$u_c = v_0 + \Phi_\mu(v_0), \quad v_0 \in \mathcal{X}_c, \quad \Phi(0, \mu_c) = 0, \quad D_{v_0} \Phi(0, \mu_c) = 0$$

to bring the reduced equation to a normal form given by:

$$\frac{dv_0}{dt} = \mathbf{A}|_{\mathcal{X}_c} v_0 + \mathbf{N}_\mu(v_0) + \rho(v_0, \mu),$$

where \mathbf{N}_μ is a polynomial of some degree p such that $\mathbf{N}_{\mu_c}(0) = 0$, $D_v \mathbf{N}_{\mu_c}(0) = 0$ and $\rho(v_0, \mu) = o(\|v_0\|^p)$. The general shape of \mathbf{N} can be guessed from symmetries for example (see [GS84,

⁹*i.e.* it gives a polynomial of degree k .

GSS88, HI10]). This nonlinear function Φ_μ is solution of a nonlinear equation which is given in [HI10]. Finally, we can combine the center manifold correction and the change of variable in one formula:

$$u = v_0 + \tilde{\Psi}(v_0, \mu), \quad \tilde{\Psi}(v_0, \mu) \equiv \Phi_\mu(v_0) + \Psi(v_0 + \Phi_\mu(v_0), \mu) \in \mathcal{Y} \quad (23)$$

where

$$\tilde{\Psi}(0, \mu_c) = 0, \quad D_{v_0} \tilde{\Psi}(0, \mu_c) = 0.$$

The nonlinear function $\tilde{\Psi}$ is solution (see [HI10, III.4.1]) of the next equations:

$$\begin{cases} D_{v_0} \tilde{\Psi}(v_0, \mu) \mathbf{A}|_{\mathcal{X}_c} v_0 - \mathbf{A} \tilde{\Psi}(v_0, \mu) + \mathbf{N}_\mu(v_0) = \mathbf{Q}(v_0) \\ \mathbf{Q}(v_0) \equiv \Pi_p \left[\mathbf{R}(v_0 + \tilde{\Psi}(v_0, \mu), \mu) - D_{v_0} \tilde{\Psi}(v_0, \mu) \mathbf{N}_\mu(v_0) \right] \end{cases} \quad (24)$$

where Π_p is the operator which takes the first $p+1$ terms in the Taylor expansion in the variable v_0 .

To sum up, when the normal form is not tabulated, then we need to solve (24) to find the normal form. In the following section, we will use tabulated formulas for the Hopf normal form. The normal form of the Fold-Hopf bifurcation and the Hopf-Hopf bifurcation with symmetries is not tabulated and we have to solve (24). To this end, we write a *Maple*© program that helps us in this task.

We will detail the computation in the case of the Pitchfork normal form. For the other normal forms, please refer to the Pitchfork normal form.

D Spectral projector

For the upcoming computation of the normal forms, we need to find the spectral projector. Its general formula was given in [VF12] and we apply it to our particular model. It is important to note that because of the equivariance of the model, the computations are greatly simplified using complex coordinates for the eigenvectors. Formally, this leads to the extension of the real history space to a complex space. The spectral projector is easy to write as a function of the following *bilinear product* between two history segments ψ, ϕ :

$$\langle\langle \psi, \phi \rangle\rangle \equiv \langle \pi_1 \psi, \pi_1 \phi \rangle_{L^2} + \int_{-\frac{\pi}{2} - \frac{\pi}{2}}^{\frac{\pi}{2}} \int_{-\frac{\pi}{2}}^{\frac{\pi}{2}} dx dy \int_{-\tau(x-y)}^0 (\pi_2 \psi)(x, -s - \tau(x-y)) J(x-y) (\pi_2 \phi)(y, s) ds.$$

We only give the expression of the spectral projector for $n > 0$; the case $n = 0$ is very similar.

Proposition D.1 *Let us consider an eigenvalue λ for the Fourier spatial mode $n > 0$ and let us assume that $1 + \sigma s_1 (J\tau e^{-\lambda\tau})_n \neq 0$. We define*

$$\beta \equiv \frac{1}{\pi(1 + \sigma s_1 (J\tau e^{-\bar{\lambda}\tau})_n)}$$

and we also write the eigenvectors with complex numbers $\phi_1 = \begin{bmatrix} e_n \\ e^{\lambda\theta} e_n \end{bmatrix}$, $\phi_2 = \begin{bmatrix} e_{-n} \\ e^{\lambda\theta} e_{-n} \end{bmatrix}$. Finally,

we define two vectors $\psi_1 = \beta \begin{bmatrix} e_n \\ e^{\bar{\lambda}\theta} e_n \end{bmatrix}$, $\psi_2 = \beta \begin{bmatrix} e_{-n} \\ e^{\bar{\lambda}\theta} e_{-n} \end{bmatrix}$. Then, we have the following results:

- the restriction of \mathbf{A} to the eigenspace associated to λ is a diagonal matrix,

- $\langle\langle\psi_i, \phi_j\rangle\rangle = \delta_{ij}$,
- the projection of any history segment $u \in C^0([-\tau_m, 0], L^2([-\frac{\pi}{2}, \frac{\pi}{2}], \mathbb{C}))$ on the eigenspace is given by

$$P_\lambda u = \sum_{i=1}^2 \langle\langle\bar{\psi}_i, u\rangle\rangle \phi_i. \quad (25)$$

- the spectral projector commutes with \mathbf{A} .

Proof. By using [VF12][prop 3.8] and arguments similar to the proof of [VF12][lemma 4.5], we show that the conditions $1 + \sigma s_1(J\tau e^{-\lambda\tau}) \neq 0$ is equivalent to $\ker(\lambda \text{Id} - \mathbf{A})^2 = \ker(\lambda \text{Id} - \mathbf{A})$ where \mathbf{A} is defined in Section B. It follows that the restriction of \mathbf{A} to the eigenspace is diagonal. The second part follows directly [VF12][prop 3.8] provided that $\langle\langle\bar{\psi}_i, \phi_j\rangle\rangle = \delta_{ij}$, which is straightforward to check. The last part is also a consequence of [VF12][prop 3.8].

E The Pitchfork bifurcation

Lemma E.1 *The pitchfork normal form coefficients $a_n^{(P)}, b_n^{(P)}$ is given by*

$$a_n^{(P)} = \pi\bar{\beta} \frac{l}{\sigma_P}, \quad b_n^{(P)} = \pi\bar{\beta} \sigma_P^3 J_n \left[\frac{s_3}{2} + \sigma_P s_2^2 \left(\frac{J_0/l}{1 - J_0/J_n} + \frac{J_{2n}/l}{2(1 - J_{2n}/J_n)} \right) \right]$$

where $\pi\beta = (1 + \sigma_P s_1(J\tau)_n)^{-1}$, $J \cdot e_n \equiv J_n e_n$, $\sigma_P = \frac{l}{s_1 J_n}$, $s_2 \equiv S_0^{(2)}(0)$ and $s_3 \equiv S_0^{(3)}(0)$.

Proof. The eigenvector $\phi = \begin{bmatrix} e_n \\ e_n \end{bmatrix}$ is associated to the eigenvalue 0 at $\sigma = \sigma_P$. The ψ vector arising on the expression of the spectral projector (25) is $\psi = \beta \begin{bmatrix} e_n \\ e_n \end{bmatrix}$ where $\pi\beta = (1 + \sigma_P s_1(J\tau)_n)^{-1}$. We write $v_0 = z\phi + \bar{z}\bar{\phi}$ and we Taylor expand the nonlinear change of variable $\tilde{\Psi}$ in (23) to bring the delayed neural field equations to the normal form (9):

$$\tilde{\Psi}(v_0, \sigma) = \sum_{l_1+l_2+r>1} z^{l_1} \bar{z}^{l_2} (\sigma - \sigma_P)^r \tilde{\Psi}_{l_1, l_2, r}, \quad \tilde{\Psi}_{l_1, l_2, r} \in \mathcal{Y},$$

where $\tilde{\Psi}$ satisfies $\tilde{\Psi}(0, \sigma_P) = 0$, $D_{v_0} \tilde{\Psi}(0, \sigma_P) = 0$ and μ is the bifurcation parameter. From [CL00, HI10], the normal form looks like:

$$\mathbf{N}_\mu = z b_n^{(P)} |z|^2 \phi + c.c. + O(|\mu - \mu_c| \cdot |z| + |z|^3) \quad (26)$$

Using the equation (24) satisfied by $\tilde{\Psi}$ and a *Maple*© program, we find the following equations. For convenience, we have indicated, in brackets, the monomials that are used to find the equation:

$$\begin{aligned} a_n \phi &= \mathbf{A} \tilde{\Psi}_{1,0,1} + \mathbf{R}_{1,0}(\phi) + 2\mathbf{R}_{2,0}(\phi, \tilde{\Psi}_{0,0,1}) & [z] \\ -2b_n^{(P)} \phi &= -2\mathbf{A} \tilde{\Psi}_{2,1,0} - 4\mathbf{R}_{2,0}(\phi, \tilde{\Psi}_{1,1,0}) - 4\mathbf{R}_{2,0}(\bar{\phi}, \tilde{\Psi}_{2,0,0}) - 6\mathbf{R}_{3,0}(\bar{\phi}, \phi, \phi) & [z^2 \bar{z}] \end{aligned}$$

where $\mathbf{R}_{ql} = \frac{1}{q!l!} \frac{\partial^{q+l}}{\partial^q u \partial^l \mu} \mathbf{R}$. For example $\mathbf{R}_{0,1} = \partial_\sigma \mathbf{R}(0, \sigma_P) = 0$. By using the spectral projector (25) which commutes with \mathbf{A} , we find:

$$\begin{aligned} a_n &= \langle\langle\bar{\psi}, \mathbf{R}_{1,0}(\phi) + 2\mathbf{R}_{2,0}(\phi, \tilde{\Psi}_{0,0,1})\rangle\rangle \\ b_n^{(P)} &= \langle\langle\bar{\psi}, 2\mathbf{R}_{2,0}(\phi, \tilde{\Psi}_{1,1,0}) + 2\mathbf{R}_{2,0}(\bar{\phi}, \tilde{\Psi}_{2,0,0}) + 3\mathbf{R}_{3,0}(\bar{\phi}, \phi, \phi)\rangle\rangle. \end{aligned}$$

In order to find the coefficients of the normal form, we are led to compute some of the coefficients of $\tilde{\Psi}$. By taking the second order monomials, we find:

$$\begin{aligned} \mathbf{A}\tilde{\Psi}_{0,0,1} &= -\mathbf{R}_{0,1} = 0 &\Rightarrow \tilde{\Psi}_{0,0,1} &= 0 \\ \mathbf{A}\tilde{\Psi}_{1,1,0} &= -2\mathbf{R}_2(\phi, \bar{\phi}) = -2\frac{\sigma_{PH}^2 s_2}{2} J_0 \begin{bmatrix} e_0 \\ 0 \end{bmatrix} &\Rightarrow \pi_2 \tilde{\Psi}_{1,1,0} &= -\frac{\sigma_{PH}^2 s_2 J_0}{-l + \sigma_{PH} s_1 J_0} e_0 + \mathbb{C}\phi + \mathbb{C}\bar{\phi} \\ \mathbf{A}\tilde{\Psi}_{2,0,0} &= -\mathbf{R}_2(\phi, \phi) = -\frac{\sigma_{PH}^2 s_2}{2} J_{2n} \begin{bmatrix} e_{2n} \\ 0 \end{bmatrix} &\Rightarrow \pi_2 \tilde{\Psi}_{2,0,0} &= -\frac{\sigma_{PH}^2 s_2}{2(-l + \sigma_{PH} s_1 J_{2n})} J_{2n} e_{2n} + \mathbb{C}\phi + \mathbb{C}\bar{\phi} \end{aligned}$$

Recall that the Ψ_{ijk} belongs to \mathcal{Y} . This is why we only give the second component of the Ψ coefficients in the above equations. Let us focus on $a_n^{(P)} = \langle \langle \bar{\psi}, \mathbf{R}_{1,0}(\phi) \rangle \rangle$. We have that $\mathbf{R}_{1,0}(\phi) = \begin{bmatrix} s_1 \mathbf{L}_1 e_n \\ 0 \end{bmatrix} = \frac{l}{\sigma_P} \begin{bmatrix} e_n \\ 0 \end{bmatrix}$ which gives the expression of $a_n^{(P)}$. The computation of $b_n^{(P)}$ is very similar.

F The $O(2)$ -Hopf bifurcation

Lemma F.1 *The coefficients are given¹⁰ by:*

$$\begin{cases} a_n^{(H)} = \pi \bar{\beta} \frac{i\omega_H + l}{\sigma_H} \\ b_n^{(H)} = \pi \bar{\beta} \frac{i\omega_H + l}{s_1} \sigma_H^2 \left[\frac{s_3}{2} + \sigma_H s_2^2 \left(\frac{J_0}{l - \sigma_H s_1 J_0} + \frac{(Je^{-2i\omega_H \tau_H})_{2n}}{2(2i\omega_H + l - \sigma_H s_1 (Je^{-2i\omega_H \tau_H})_{2n})} \right) \right] \\ c_n^{(H)} = \pi \bar{\beta} \frac{i\omega_H + l}{s_1} \sigma_H^2 \left[s_3 + \sigma_H s_2^2 \left(\frac{J_0}{l - \sigma_H s_1 J_0} + \frac{J_{2n}}{l - \sigma_H s_1 J_{2n}} + \frac{(Je^{-2i\omega_H \tau_H})_0}{2i\omega_H + l - \sigma_H s_1 (Je^{-2i\omega_H \tau_H})_0} \right) \right] \end{cases}$$

with $\bar{\beta}^{-1} = \pi(1 + s_1 \sigma_H (J\tau_H e^{-i\omega_H \tau_H})_n)$.

Proof. The two eigenvectors for the eigenvalue $i\omega_H$ are $\phi_1 = \begin{bmatrix} e_n \\ e^{i\omega_H \theta} e_n \end{bmatrix}$, $\phi_2 = \begin{bmatrix} e_{-n} \\ e^{i\omega_H \theta} e_{-n} \end{bmatrix}$. According to the expression of the spectral projector (25), we need to define two additional vectors $\psi_1 = \beta \begin{bmatrix} e_n \\ e^{-i\omega_H \theta} e_n \end{bmatrix}$, $\phi = \beta_2 \begin{bmatrix} e_{-n} \\ e^{-i\omega_H \theta} e_{-n} \end{bmatrix}$ with $\bar{\beta}^{-1} = \pi(1 + s_1 \sigma_H (J\tau_H e^{-i\omega_H \tau_H})_n)$. The bifurcation is studied in [HI10] where it is shown that:

$$\begin{cases} a_n^{(H)} = \langle \langle \bar{\psi}_1, \mathbf{R}_{11}(\phi_1) + 2\mathbf{R}_{20}(\phi_1, \Psi_{00001}) \rangle \rangle \\ b_n^{(H)} = \langle \langle \bar{\psi}_1, 3\mathbf{R}_{30}(\phi_1, \phi_1, \bar{\phi}_1) + 2\mathbf{R}_{20}(\bar{\phi}_1, \Psi_{20000}) + 2\mathbf{R}_{20}(\phi_1, \Psi_{11000}) \rangle \rangle \\ c_n^{(H)} = \langle \langle \bar{\psi}_1, 6\mathbf{R}_{30}(\phi_1, \phi_2, \bar{\phi}_2) + 2\mathbf{R}_{20}(\phi_1, \Psi_{00110}) + 2\mathbf{R}_{20}(\phi_2, \Psi_{10010}) + 2\mathbf{R}_{20}(\bar{\phi}_2, \Psi_{10100}) \rangle \rangle \end{cases}$$

with $\mathbf{R}_{ql} = \frac{1}{q!l!} \frac{\partial^{q+l}}{\partial^q u \partial^l \mu} \mathbf{R}$. Let us write the nonlinear change of variable $\tilde{\Psi}$ to bring the delayed neural field equations to the normal form (9). We Taylor expand $\tilde{\Psi}$:

$$\tilde{\Psi}(v_0, \mu) = \sum_{l_1+l_2+r>1} z^{l_1} \bar{z}^{l_2} (\mu - \mu_c)^r \tilde{\Psi}_{l_1, l_2, r}, \quad \tilde{\Psi}_{l_1, l_2, r} \in \mathcal{Y},$$

where $\tilde{\Psi}$ satisfies $\tilde{\Psi}(0, \mu_c) = 0$, $D_{v_0} \tilde{\Psi}(0, \mu_c) = 0$ and μ is the bifurcation parameter. The equations for the $\tilde{\Psi}$ coefficients are also given in [HI10]. They are solved below and we only show

¹⁰Recall that $(Je^{-2i\omega_H \tau_H})_n \equiv \int Je^{-2i\omega_H \tau_H} \cos n$.

how to solve one of them.

$$\left\{ \begin{array}{ll} \mathbf{A}\tilde{\Psi}_{00001} = -\mathbf{R}_{01} = 0 & \Rightarrow \pi_2\tilde{\Psi}_{00001} = 0 \\ (2i\omega_H - \mathbf{A})\tilde{\Psi}_{20000} = \mathbf{R}_{20}(\phi_1, \phi_1) & \Rightarrow \pi_2\tilde{\Psi}_{20000} = \sigma_H^2 s_2 \frac{(Je^{-2i\omega_H\tau})_{2n}}{2(2i\omega_H + l - \sigma_H s_1 (Je^{-2i\omega_H\tau})_{2n})} e^{2i\omega_H\theta} e_{2n} \\ \mathbf{A}\tilde{\Psi}_{11000} = -2\mathbf{R}_{20}(\phi_1, \bar{\phi}_1) & \Rightarrow \pi_2\tilde{\Psi}_{11000} = \sigma_H^2 s_2 \frac{-J_0}{-l + \sigma_H s_1 J_0} e_0 \\ (2i\omega_H - \mathbf{A})\tilde{\Psi}_{10100} = 2\mathbf{R}_{20}(\phi_1, \phi_2) & \Rightarrow \pi_2\tilde{\Psi}_{10100} = \sigma_H^2 s_2 \frac{(Je^{-2i\omega_H\tau})_0}{2i\omega_H + l - \sigma_H s_1 (Je^{-2i\omega_H\tau})_0} e^{2i\omega_H\theta} e_0 \\ \mathbf{A}\tilde{\Psi}_{10010} = -2\mathbf{R}_{20}(\phi_1, \bar{\phi}_2) & \Rightarrow \pi_2\tilde{\Psi}_{10010} = \sigma_H^2 s_2 \frac{-J_{2n}}{-l + \sigma_H^2 s_2 J_{2n}} e_{2n} \\ \tilde{\Psi}_{00110} = S \cdot \tilde{\Psi}_{11000} \text{ (reflection)} & \Rightarrow \tilde{\Psi}_{00110} = \tilde{\Psi}_{11000} \end{array} \right.$$

Recall that the Ψ_{ijklm} belongs to \mathcal{Y} . This is why we only give the second component of the Ψ coefficients in the above equations. Let us show, for example, how to solve the second equation $(2i\omega_H - \mathbf{A})\Psi_{20000} = \mathbf{R}_{20}(\phi_1, \phi_1)$. From $(2i\omega_H - \frac{d}{d\theta})\pi_2\Psi_{20000} = 0$, we find that $(\pi_2\Psi_{20000})(\theta) = (\pi_1\Psi_{20000})e^{2i\omega_H\theta}$. Using $\mathbf{R}_{20}(\phi_1, \phi_1) = \begin{bmatrix} \frac{s_2}{2}(Je^{-2i\omega_H\tau})_{2n}e_{2n} \\ 0 \end{bmatrix}$, the equation for the first component is:

$$\frac{s_2}{2}(Je^{-2i\omega_H\tau})_{2n}e_{2n} = (2i\omega_H + l - \sigma_H s_1 J(2i\omega_H))\pi_1\Psi_{20000}$$

This convolutional equation shows that Ψ_{20000} is collinear to e_{2n} which then gives the solution:

$$\pi_2\Psi_{20000} = \sigma_H^2 s_2 \frac{(Je^{-2i\omega_H\tau})_{2n}}{2(2i\omega_H + l - \sigma_H s_1 (Je^{-2i\omega_H\tau})_{2n})} e^{2i\omega_H\theta} e_{2n}.$$

The expressions for $b_n^{(H)}, c_n^{(H)}$ follow easily. Let us compute $a_n^{(H)} = \langle \langle \bar{\psi}_1, \mathbf{R}_{1,0}(\phi_1) \rangle \rangle$. We have $\mathbf{R}_{0,1}(\phi_1) = \begin{bmatrix} s_1 \mathbf{L}_1 \phi_1 \\ 0 \end{bmatrix} = \frac{i\omega_H + l}{\sigma_H} \begin{bmatrix} e_n \\ 0 \end{bmatrix}$ which gives the expression of $a_n^{(H)}$.

G Pitchfork-Hopf bifurcation

Lemma G.1 *The Pitchfork-Hopf normal form truncated at cubic order:*

$$\begin{cases} \dot{z}_1 &= \left(a_1 + b_n^{(P)}|z_1|^2 + c_{(1)}^{(PH)}|z_2|^2 \right) z_1 \\ \dot{z}_2 &= \left(i\omega_{PH} + a_2 + b_0^{(H)}|z_2|^2 + c_{(2)}^{(PH)}|z_1|^2 \right) z_2 \end{cases}$$

has the following coefficients:

$$\left\{ \begin{array}{l} \frac{a_1}{\pi\beta_1} = \frac{l_{PH}}{\sigma_{PH}}(\sigma - \sigma_{PH}) - (l - l_{PH}) \\ \frac{a_2}{\pi\beta_2} = \frac{l_{PH} + i\omega_{PH}}{\sigma_{PH}}(\sigma - \sigma_{PH}) - (l - l_{PH}) \\ \frac{c_{(1)}^{(PH)}}{\pi\beta_1} = \sigma_{PH}^3 J_n \left[s_3 + \sigma_{PH} s_2^2 \left(\frac{J_0/l}{1 - J_0/J_n} + \frac{(Je^{-i\omega_{PH}\tau_{PH}})_n}{i\omega_{PH} + l - l(Je^{-i\omega_{PH}\tau_{PH}})_n/J_n} + \frac{(Je^{i\omega_{PH}\tau_{PH}})_n}{-i\omega_{PH} + l - l(Je^{i\omega_{PH}\tau_{PH}})_n/J_n} \right) \right] \\ \frac{c_{(2)}^{(PH)}}{\pi\beta_2} = (i\omega_{PH} + 1) \frac{J_n}{l} \sigma_{PH}^3 \left[s_3 + \sigma_{PH} s_2^2 \left(\frac{J_0/l}{1 - J_0/J_n} + 2 \frac{(Je^{-i\omega_{PH}\tau_{PH}})_n}{i\omega_{PH} + l - l(Je^{-i\omega_{PH}\tau_{PH}})_n/J_n} \right) \right] \end{array} \right.$$

where $J \cdot e_n \equiv J_n e_n$, $\sigma_{PH} = \frac{l}{s_1 J_n}$, $(Je^{-i\omega_{PH}\tau_{PH}})_0 = \frac{i\omega_{PH} + l}{\sigma_{PH} s_1} = (i\omega_{PH} + l) \frac{J_n}{l}$, $s_2 \equiv S_0^{(2)}(0)$, $s_3 \equiv S_0^{(3)}(0)$ and $\bar{\beta}_1^{-1} = \pi + \pi\sigma_{PH} s_1 (J\tau)_n \in \mathbb{R}$, $\bar{\beta}_2^{-1} = \pi + \pi\sigma_{PH} s_1 (J\tau e^{-i\omega_{PH}\tau})_0$.

Proof.

Here, we have two eigenvectors for the eigenvalues 0 and $i\omega_{PH}$. We also give the expression of the vectors needed for the computation of the spectral projector:

$$\phi_1 = \begin{bmatrix} e_n \\ e_n \end{bmatrix}, \quad \phi_2 = \begin{bmatrix} e_0 \\ e^{i\omega_{PH}\theta} e_0 \end{bmatrix}, \quad \psi_1 = \beta_1 \phi_1, \quad \psi_2 = \beta_2 \begin{bmatrix} e_0 \\ e^{-i\omega_{PH}\theta} e_0 \end{bmatrix}$$

with $\bar{\beta}_1^{-1} = \pi + \pi\sigma_{PH} s_1(J\tau)_n \in \mathbb{R}$, $\bar{\beta}_2^{-1} = \pi + \pi\sigma_{PH} s_1(J\tau e^{-i\omega_{PH}\tau})_0$. We write $v_0 = z_1\phi_1 + z_2\phi_2 + c.c.$ (complex conjugate) and we Taylor expand the nonlinear change of variable $\tilde{\Psi}$ in (23) to bring the delayed neural field equations to the normal form (13):

$$\tilde{\Psi}(v_0, \mu) = \sum_{l_1+l_2+p_1+p_2+r>1} z_1^{l_1} \bar{z}_1^{l_2} z_2^{p_1} \bar{z}_2^{p_2} (\mu - \mu_c)^r \tilde{\Psi}_{l_1, l_2, p_1, p_2, r}, \quad \tilde{\Psi}_{l_1, l_2, p_1, p_2, r} \in \mathcal{Y},$$

where $\tilde{\Psi}$ satisfies $\tilde{\Psi}(0, \mu_c) = 0$, $D_{v_0} \tilde{\Psi}(0, \mu_c) = 0$. There is an abuse of notation in the previous Taylor expansion as in the present case $\mu = (\sigma, l)$. Using the equation (24) satisfied by $\tilde{\Psi}$ and a *Maple*[®] program, we find the following equations. For convenience, we have indicated, in brackets, the monomials that are used to find the equation. We need to be more precise for the expression of the a_k to give the equation they satisfy:

$$\begin{aligned} a_1 &\equiv a_1^{(1)}(\sigma - \sigma_{PH}) + a_1^{(2)}(l - l_{PH}) \\ a_2 &\equiv a_2^{(1)}(\sigma - \sigma_{PH}) + a_2^{(2)}(l - l_{PH}), \end{aligned}$$

then we find

$$\begin{aligned} -a_1^{(k)} \phi_1 &= -\mathbf{A} \tilde{\Psi}_{1,0,0,0,1} - \mathbf{R}_{0,1}(\phi_1) - 2\mathbf{R}_2(\phi_1, \tilde{\Psi}_{0,0,0,0,1}) & [z_1] \\ -a_2^{(k)} \phi_2 &= (i\omega_{PH} - \mathbf{A}) \tilde{\Psi}_{0,0,1,0,1} - \mathbf{R}_{0,1}(\phi_2) - 2\mathbf{R}_2(\phi_2, \tilde{\Psi}_{0,0,0,0,1}) & [z_2] \\ -c_{(2)}^{(PH)} \phi_2 &= (i\omega_{PH} - \mathbf{A}) \tilde{\Psi}_{1,1,1,0,0} - 2\mathbf{R}_2(\tilde{\Psi}_{0,1,1,0,0}, \phi_1) \\ &\quad - 2\mathbf{R}_2(\bar{\phi}_1, \tilde{\Psi}_{1,0,1,0,0}) - 2\mathbf{R}_2(\phi_2, \tilde{\Psi}_{1,1,0,0,0}) - 6\mathbf{R}_3(\phi_2, \phi_1, \bar{\phi}_1) & [z_1 \bar{z}_1 z_2] \\ -c_{(1)}^{(PH)} \phi_1 &= -2\mathbf{A} \tilde{\Psi}_{1,0,1,1,0} - 2\mathbf{R}_2(\tilde{\Psi}_{1,0,0,1,0}, \phi_2) \\ &\quad - 2\mathbf{R}_2(\bar{\phi}_2, \tilde{\Psi}_{1,0,1,0,0}) - 2\mathbf{R}_2(\phi_1, \tilde{\Psi}_{0,0,1,1,0}) - 6\mathbf{R}_3(\phi_2, \phi_1, \bar{\phi}_2) & [z_2 \bar{z}_2 z_1] \end{aligned}$$

Then, by using the spectral projector (25) which commutes with \mathbf{A} , we find:

$$\begin{aligned} a_1^{(k)} &= \langle \langle \bar{\psi}_1, \mathbf{R}_{0,1}(\phi_1) + 2\mathbf{R}_2(\phi_1, \tilde{\Psi}_{0,0,0,0,1}) \rangle \rangle \\ a_2^{(k)} &= \langle \langle \bar{\psi}_2, \mathbf{R}_{0,1}(\phi_2) + 2\mathbf{R}_2(\phi_2, \tilde{\Psi}_{0,0,0,0,1}) \rangle \rangle \\ c_{(2)}^{(PH)} &= \langle \langle \bar{\psi}_2, 2\mathbf{R}_2(\tilde{\Psi}_{0,1,1,0,0}, \phi_1) + 2\mathbf{R}_2(\bar{\phi}_1, \tilde{\Psi}_{1,0,1,0,0}) + 2\mathbf{R}_2(\phi_2, \tilde{\Psi}_{1,1,0,0,0}) \\ &\quad + 6\mathbf{R}_3(\phi_2, \phi_1, \bar{\phi}_1) \rangle \rangle \\ c_{(1)}^{(PH)} &= \langle \langle \bar{\psi}_1, 2\mathbf{R}_2(\tilde{\Psi}_{1,0,0,1,0}, \phi_2) + 2\mathbf{R}_2(\bar{\phi}_2, \tilde{\Psi}_{1,0,1,0,0}) + 2\mathbf{R}_2(\phi_1, \tilde{\Psi}_{0,0,1,1,0}) \\ &\quad + 6\mathbf{R}_3(\phi_2, \phi_1, \bar{\phi}_2) \rangle \rangle \end{aligned}$$

where $\mathbf{R}_{ql} = \frac{1}{q!l!} \frac{\partial^{q+l}}{\partial^q u \partial^l \mu} \mathbf{R}$. In order to find the coefficients of the normal form, we are led to compute some of the coefficients of $\tilde{\Psi}$. By taking the second order monomials, we find (we omit

the part in the nullspace for simplicity):

$$\begin{aligned}
\mathbf{A}\tilde{\Psi}_{0,0,0,0,1} = 0 & \Rightarrow \pi_2\tilde{\Psi}_{0,0,0,0,1} \in \mathbb{C}\phi_1 \\
\mathbf{A}\tilde{\Psi}_{1,1,0,0,0} & = -2\mathbf{R}_2(\phi_1, \bar{\phi}_1) = -2\frac{\sigma_{PH}^2 s_2}{2} J_0 \begin{bmatrix} e_0 \\ 0 \end{bmatrix} \\
& \Rightarrow \pi_2\tilde{\Psi}_{1,1,0,0,0} = -\frac{\sigma_{PH}^2 s_2 J_0}{-l + \sigma_{PH} s_1 J_0} e_0 \\
(i\omega_{PH} - \mathbf{A})\tilde{\Psi}_{1,0,1,0,0} & = 2\mathbf{R}_2(\phi_1, \phi_2) = 2\frac{\sigma_{PH}^2 s_2}{2} (Je^{-i\omega_{PH}\tau_{PH}})_n \begin{bmatrix} e_n \\ 0 \end{bmatrix} \\
& \Rightarrow \pi_2\tilde{\Psi}_{1,0,1,0,0} = \frac{\sigma_{PH}^2 s_2 (Je^{-i\omega_{PH}\tau_{PH}})_n}{i\omega_{PH} + l - \sigma_{PH} s_1 (Je^{-i\omega_{PH}\tau_{PH}})_n} e_n e^{i\omega_H \theta} \\
\mathbf{A}\tilde{\Psi}_{0,0,1,1,0} & = -2\mathbf{R}_2(\phi_2, \bar{\phi}_2) = -2\frac{\sigma_{PH}^2 s_2 J_0}{2} \begin{bmatrix} e_0 \\ 0 \end{bmatrix} \\
& \Rightarrow \pi_2\tilde{\Psi}_{0,0,1,1,0} = -\frac{\sigma_{PH}^2 s_2 J_0}{-l + \sigma_{PH} s_1 J_0} e_0 \\
(i\omega_{PH} + \mathbf{A})\tilde{\Psi}_{1,0,0,1,0} & = -2\mathbf{R}_2(\phi_1, \bar{\phi}_2) = -2\frac{\sigma_{PH}^2 s_2}{2} (Je^{i\omega_{PH}\tau_{PH}})_n \begin{bmatrix} e_n \\ 0 \end{bmatrix} \\
& \Rightarrow \pi_2\tilde{\Psi}_{1,0,0,1,0} = \frac{-\sigma_{PH}^2 s_2 (Je^{i\omega_{PH}\tau_{PH}})_n}{i\omega_{PH} - l + \sigma_{PH} s_1 (Je^{i\omega_{PH}\tau_{PH}})_n} e_n e^{-i\omega_{PH}\theta} \\
(i\omega_{PH} - \mathbf{A})\tilde{\Psi}_{0,1,1,0,0} & = 2\mathbf{R}_2(\phi_2, \bar{\phi}_1) = 2\frac{\sigma_{PH}^2 s_2}{2} (Je^{-i\omega_{PH}\tau_{PH}})_{-n} \begin{bmatrix} e_{-n} \\ 0 \end{bmatrix} \\
& \Rightarrow \pi_2\tilde{\Psi}_{0,1,1,0,0} = \frac{\sigma_{PH}^2 s_2 (Je^{-i\omega_{PH}\tau_{PH}})_{-n}}{i\omega_{PH} + l - \sigma_{PH} s_1 (Je^{-i\omega_{PH}\tau_{PH}})_{-n}} e_{-n} e^{i\omega_{PH}\theta}
\end{aligned}$$

Let us just indicate how to solve the third equation $(i\omega_{PH} - \mathbf{A})\tilde{\Psi}_{1,0,1,0,0} = 2\mathbf{R}_2(\phi_1, \phi_2)$. The second component of the equation: $(i\omega_{PH} - \frac{d}{d\theta})\pi_2\tilde{\Psi}_{1,0,1,0,0} = 0$ gives $\pi_2\tilde{\Psi}_{1,0,1,0,0} = \pi_1\tilde{\Psi}_{1,0,1,0,0}e^{i\omega_{PH}\theta}$. If we insert this solution in the first component of the equation, we find:

$$(i\omega_{PH} + l - \sigma_{PH} s_1 J(i\omega_{PH}))\pi_1\tilde{\Psi}_{1,0,1,0,0} = 2\frac{\sigma_{PH}^2 s_2}{2} (Je^{-i\omega_{PH}\tau_{PH}})_n e_n.$$

The kernel is $\ker(i\omega_{PH} + l - \sigma_{PH} s_1 J(i\omega_{PH})) = \mathbb{C}e_0$ and we find: $\pi_2\tilde{\Psi}_{1,0,1,0,0}(\theta) = \frac{\sigma_{PH}^2 s_2 (Je^{-i\omega_{PH}\tau_{PH}})_n}{i\omega_{PH} + l - \sigma_{PH} s_1 (Je^{-i\omega_{PH}\tau_{PH}})_n} e_n \mathbb{C}e_0 e^{i\omega_{PH}\theta}$.

Let us also show how to compute a_1 . We find that $a_1^{(k)} = \langle \langle \bar{\psi}_1, \mathbf{R}_{0,1}(\phi_1), \tilde{\Psi}_{0,0,0,0,1} \rangle \rangle$. The expression of $a_1^{(1)}$ is similar to the case of the Hopf bifurcation so we do not reproduce the computations. For $a_1^{(2)}$, we have (derivative w.r.t. l) $\mathbf{R}_{0,1}(\phi_1) = \begin{bmatrix} -e_n \\ 0 \end{bmatrix}$ which gives $a_1^{(2)} = -\pi\bar{\beta}_1$.

Using the previous formulas and $J \cdot e_n \equiv J_n e_n$, $\sigma_{PH} = \frac{l}{s_1 J_n}$, $(Je^{-i\omega_{PH}\tau_{PH}})_0 = \frac{i\omega_{PH} + l}{\sigma_{PH} s_1} = (i\omega_{PH} + l)J_n/l$, it is straightforward to obtain the lemma.

H Hopf-Hopf normal form, 6d case

Lemma H.1 *The Hopf-Hopf $0 : n$ normal form truncated at cubic order*

$$\begin{cases} \dot{z}_0 = z_0 \left(i\omega_0 + a_0 + b_0^{(H)} |z_0|^2 + c_{(0)}^{(HH)} (|z_1|^2 + |z_2|^2) \right) \\ \dot{z}_1 = z_1 \left(i\omega_1 + a_1 + b_{(1)}^{(HH)} |z_0|^2 + b_n^{(H)} |z_1|^2 + c_n^{(H)} |z_2|^2 \right) \\ \dot{z}_2 = z_2 \left(i\omega_1 + a_1 + b_{(1)}^{(HH)} |z_0|^2 + c_n^{(H)} |z_1|^2 + b_n^{(H)} |z_2|^2 \right) \end{cases} \quad (27)$$

Inria

has the following coefficients:

$$\begin{aligned} c_{(0)}^{(HH)} &= \pi \bar{\beta}_0 \frac{i\omega_0 + l}{s_1} \sigma_{HH}^2 \left[s_3 + \sigma_{HH} s_2^2 \left(\frac{J_0}{l - \sigma_{HH} s_1 J_0} + \frac{(Je^{-i(\omega_0 - \omega_1)\tau})_n}{i(\omega_0 - \omega_1) + l - \sigma_{HH} s_1 (Je^{-i(\omega_0 - \omega_1)\tau})_n} + \frac{(Je^{-i(\omega_0 + \omega_1)\tau})_n}{i(\omega_0 + \omega_1) + l - \sigma_{HH} s_1 (Je^{-i(\omega_0 + \omega_1)\tau})_n} \right) \right] \\ b_{(1)}^{(HH)} &= \pi \bar{\beta}_1 \frac{i\omega_1 + l}{s_1} \sigma_{HH}^2 \left[s_3 + \sigma_{HH} s_2^2 \left(\frac{J_0}{l - \sigma_{HH} s_1 J_0} + \frac{(Je^{-i(\omega_1 - \omega_0)\tau})_n}{i(\omega_1 - \omega_0) + l - \sigma_{HH} s_1 (Je^{-i(\omega_1 - \omega_0)\tau})_n} + \frac{(Je^{-i(\omega_1 + \omega_0)\tau})_n}{i(\omega_1 + \omega_0) + l - \sigma_{HH} s_1 (Je^{-i(\omega_1 + \omega_0)\tau})_n} \right) \right] \end{aligned}$$

where $J \cdot e_n \equiv J_n e_n$, $(Je^{-i\omega_0\tau_{HH}})_0 = \frac{i\omega_0 + l}{\sigma_{HH} s_1}$, $(Je^{-i\omega_1\tau_{HH}})_n = \frac{i\omega_1 + l}{\sigma_{HH} s_1}$ and $s_2 \equiv S_0^{(2)}(0)$, $s_3 \equiv S_0^{(3)}(0)$.

Proof. We write the eigenvectors

$$\phi_0 = \begin{bmatrix} e_0 \\ e^{i\omega_0\theta} e_0 \end{bmatrix}, \quad \phi_1 = \begin{bmatrix} e_n \\ e^{i\omega_1\theta} e_n \end{bmatrix}, \quad \phi_2 = \begin{bmatrix} e_{-n} \\ e^{i\omega_1\theta} e_{-n} \end{bmatrix},$$

and the associated vectors for the spectral projector (25):

$$\psi_0 = \beta_0 \begin{bmatrix} e_0 \\ e^{-i\omega_0\theta} e_0 \end{bmatrix}, \quad \psi_1 = \beta_1 \begin{bmatrix} e_n \\ e^{-i\omega_1\theta} e_n \end{bmatrix}, \quad \psi_2 = \beta_2 \begin{bmatrix} e_{-n} \\ e^{-i\omega_1\theta} e_{-n} \end{bmatrix}$$

where the normalization factors satisfy $\bar{\beta}_k^{-1} = \pi + \pi s_1 \sigma_{HH} (J \tau_{HH} e^{-i\omega_k \tau_H})_{|n_k|}$, $k = 0, 1, 2$ with $(n_0, n_1, n_2) = (0, n, -n)$. Using the same procedure as for the other normal forms, we find the next equations. Using the equation (24) satisfied by $\tilde{\Psi}$ and a *Maple*[©] program, we have:

$$\begin{aligned} 0 &= (i\omega_0 - \mathbf{A}) \tilde{\Psi}_{1,0,1,1,0,0,0} + c_{(0)}^{(HH)} \phi_0 - 2\mathbf{R}_2(\tilde{\Psi}_{1,0,0,1,0,0,0}, \phi_1) - 2\mathbf{R}_2(\bar{\phi}_1, \tilde{\Psi}_{1,0,1,0,0,0,0}) \\ &\quad - 2\mathbf{R}_2(\phi_0, \tilde{\Psi}_{0,0,1,1,0,0,0}) - 6\mathbf{R}_3(\phi_0, \phi_1, \bar{\phi}_1) \\ 0 &= (i\omega_1 - \mathbf{A}) \tilde{\Psi}_{1,1,1,0,0,0,0} + b_{(1)}^{(HH)} \phi_1 - 2\mathbf{R}_2(\tilde{\Psi}_{0,1,1,0,0,0,0}, \phi_0) - 2\mathbf{R}_2(\bar{\phi}_0, \tilde{\Psi}_{1,0,1,0,0,0,0}) \\ &\quad - 2\mathbf{R}_2(\phi_1, \tilde{\Psi}_{1,1,0,0,0,0,0}) - 6\mathbf{R}_3(\phi_1, \phi_0, \bar{\phi}_0) \end{aligned}$$

Then, by using the spectral projector (25) which commutes with \mathbf{A} , we find:

$$\begin{aligned} c_{(0)}^{(HH)} &= \langle \langle \bar{\psi}_0, 2\mathbf{R}_2(\tilde{\Psi}_{1,0,0,1,0,0,0}, \phi_1) + 2\mathbf{R}_2(\bar{\phi}_1, \tilde{\Psi}_{1,0,1,0,0,0,0}) + 2\mathbf{R}_2(\phi_0, \tilde{\Psi}_{0,0,1,1,0,0,0}) \\ &\quad + 6\mathbf{R}_3(\phi_0, \phi_1, \bar{\phi}_1) \rangle \rangle \\ b_{(1)}^{(HH)} &= \langle \langle \bar{\psi}_1, 2\mathbf{R}_2(\tilde{\Psi}_{0,1,1,0,0,0,0}, \phi_0) + 2\mathbf{R}_2(\bar{\phi}_0, \tilde{\Psi}_{1,0,1,0,0,0,0}) + 2\mathbf{R}_2(\phi_1, \tilde{\Psi}_{1,1,0,0,0,0,0}) \\ &\quad + 6\mathbf{R}_3(\phi_1, \phi_0, \bar{\phi}_0) \rangle \rangle \end{aligned}$$

where $\mathbf{R}_{ql} = \frac{1}{q!l!} \frac{\partial^{q+l}}{\partial^q u \partial^l \mu} \mathbf{R}$. In order to find the coefficients of the normal form, we are led to compute some of the coefficients of $\tilde{\Psi}$. By taking the second order terms, we find the next

equations. As above, we omit the part in the nullspace.

$$\begin{aligned}
\mathbf{A}\tilde{\Psi}_{1100000} &= -2\mathbf{R}_2(\bar{\phi}_0, \phi_0) \\
&= -2\frac{\sigma_{HH}^2 s_2}{2} J_0 \begin{bmatrix} e_0 \\ 0 \end{bmatrix} \Rightarrow \pi_2 \tilde{\Psi}_{1100000} = -\frac{\sigma_{HH}^2 s_2 J_0}{-l + \sigma_{HH} s_1 J_0} e_0 \\
(i\omega_0 - i\omega_1 - \mathbf{A})\tilde{\Psi}_{1001000} &= 2\mathbf{R}_2(\bar{\phi}_1, \phi_0) \\
&= \sigma_{HH}^2 s_2 (Je^{-i(\omega_0 - \omega_1)\tau})_n \begin{bmatrix} e_{-n} \\ 0 \end{bmatrix} \\
&\Rightarrow \pi_2 \tilde{\Psi}_{1001000} = \frac{\sigma_{HH}^2 s_2 (Je^{-i(\omega_0 - \omega_1)\tau})_n e^{i(\omega_0 - \omega_1)\theta}}{i(\omega_0 - \omega_1) + l - \sigma_{HH} s_1 (Je^{-i(\omega_0 - \omega_1)\tau})_n} e_{-n} \\
(i\omega_1 + i\omega_0 - \mathbf{A})\tilde{\Psi}_{1010000} &= 2\mathbf{R}_2(\phi_1, \phi_0) \\
&= 2\frac{\sigma_{HH}^2 s_2}{2} (Je^{-i(\omega_0 + \omega_1)\tau})_n \begin{bmatrix} e_n \\ 0 \end{bmatrix} \\
&\Rightarrow \pi_2 \tilde{\Psi}_{1010000} = \frac{\sigma_{HH}^2 s_2 (Je^{-i(\omega_0 + \omega_1)\tau})_n e^{i(\omega_0 + \omega_1)\theta}}{i(\omega_0 + \omega_1) + l - \sigma_{HH} s_1 (Je^{-i(\omega_0 + \omega_1)\tau})_n} e_n \\
\mathbf{A}\tilde{\Psi}_{0011000} &= -2\mathbf{R}_2(\bar{\phi}_1, \phi_1) \\
&= -2\frac{\sigma_{HH}^2 s_2}{2} J_0 \begin{bmatrix} e_0 \\ 0 \end{bmatrix} \Rightarrow \pi_2 \tilde{\Psi}_{0011000} = -\frac{\sigma_{HH}^2 s_2 J_0}{-l + \sigma_{HH} s_1 J_0} e_0 \\
(i\omega_1 - i\omega_0 - \mathbf{A})\tilde{\Psi}_{0110000} &= 2\mathbf{R}_2(\phi_1, \bar{\phi}_0) \\
&= 2\frac{\sigma_{HH}^2 s_2}{2} (Je^{-i(\omega_1 - \omega_0)\tau})_n \begin{bmatrix} e_n \\ 0 \end{bmatrix} \\
&\Rightarrow \pi_2 \tilde{\Psi}_{0110000} = \frac{\sigma_{HH}^2 s_2 (Je^{-i(\omega_1 - \omega_0)\tau})_n e^{i(\omega_1 - \omega_0)\theta}}{i(\omega_1 - \omega_0) + l - \sigma_{HH} s_1 (Je^{-i(\omega_1 - \omega_0)\tau})_n} e_n.
\end{aligned}$$

It is then straightforward to obtain the lemma.

I Hopf-Hopf normal form, 8d case

Lemma I.1 *The Hopf-Hopf $p : q$ normal form truncated at cubic order*

$$\begin{cases} \dot{z}_1 = z_1 \left(i\omega_p + a_1 + b_p^{(H)} |z_1|^2 + c_p^{(H)} |z_2|^2 + d_{(1)}^{(HH)} |z_3|^2 + e_{(1)}^{(HH)} |z_4|^2 \right) \\ \dot{z}_2 = z_2 \left(i\omega_p + a_1 + b_p^{(H)} |z_2|^2 + c_p^{(H)} |z_1|^2 + d_{(1)}^{(HH)} |z_4|^2 + e_{(1)}^{(HH)} |z_3|^2 \right) \\ \dot{z}_3 = z_3 \left(i\omega_q + a_3 + b_{(3)}^{(HH)} |z_1|^2 + c_{(3)}^{(HH)} |z_2|^2 + b_q^{(H)} |z_3|^2 + c_q^{(H)} |z_4|^2 \right) \\ \dot{z}_4 = z_4 \left(i\omega_q + a_3 + b_{(3)}^{(HH)} |z_2|^2 + c_{(3)}^{(HH)} |z_1|^2 + b_q^{(H)} |z_4|^2 + c_q^{(H)} |z_3|^2 \right) \end{cases} \quad (28)$$

has the following coefficients:

$$\begin{aligned}
d_{(1)}^{(HH)} / \pi \bar{\beta}_1 &= \frac{i\omega_p + l}{s_1} \sigma_{HH}^2 \left[s_3 + \sigma_{HH} s_2^2 \left(\frac{J_0}{l - s_1 \sigma_{HH} J_0} + \frac{(Je^{-i(\omega_p - \omega_q)\tau})_{p-q}}{-i\omega_q + i\omega_p + l - \sigma_{HH} s_1 (Je^{-i(\omega_p - \omega_q)\tau})_{p-q}} \right. \right. \\
&\quad \left. \left. + \frac{(Je^{-i(\omega_p + \omega_q)\tau})_{p+q}}{i\omega_q + i\omega_p + l - \sigma_{HH} s_1 (Je^{-i(\omega_p + \omega_q)\tau})_{p+q}} \right) \right] \\
e_{(1)}^{(HH)} / \pi \bar{\beta}_1 &= \frac{i\omega_p + l}{s_1} \sigma_{HH}^2 \left[s_3 + \sigma_{HH} s_2^2 \left(\frac{J_0}{l - s_1 \sigma_{HH} J_0} + \frac{(Je^{-i(\omega_p - \omega_q)\tau})_{p+q}}{-i\omega_q + i\omega_p + l - \sigma_{HH} s_1 (Je^{-i(\omega_p - \omega_q)\tau})_{p+q}} \right. \right. \\
&\quad \left. \left. + \frac{(Je^{-i(\omega_p + \omega_q)\tau})_{p-q}}{i\omega_q + i\omega_p + l - \sigma_{HH} s_1 (Je^{-i(\omega_p + \omega_q)\tau})_{p-q}} \right) \right]
\end{aligned}$$

$$b_{(3)}^{(HH)} / \pi \overline{\beta_2} = \frac{i\omega_q + l}{s_1} \sigma_{HH}^2 \left[s_3 + \sigma_{HH} s_2^2 \left(\frac{J_0}{l - s_1 \sigma_{HH} J_0} + \frac{(J e^{-i(\omega_q - \omega_p)\tau})_{p-q}}{i\omega_q - i\omega_p + l - \sigma_{HH} s_1 (J e^{-i(\omega_q - \omega_p)\tau})_{p-q}} \right. \right. \\ \left. \left. + \frac{(J e^{-i(\omega_p + \omega_q)\tau})_{p+q}}{i\omega_q + i\omega_p + l - \sigma_{HH} s_1 (J e^{-i(\omega_p + \omega_q)\tau})_{p+q}} \right) \right]$$

$$c_{(3)}^{(HH)} / \pi \overline{\beta_2} = \frac{i\omega_q + l}{s_1} \sigma_{HH}^2 \left[s_3 + \sigma_{HH} s_2^2 \left(\frac{J_0}{l - s_1 \sigma_{HH} J_0} + \frac{(J e^{-i(\omega_q - \omega_p)\tau})_{p+q}}{i\omega_q - i\omega_p + l - \sigma_{HH} s_1 (J e^{-i(\omega_q - \omega_p)\tau})_{p+q}} \right. \right. \\ \left. \left. + \frac{(J e^{-i(\omega_p + \omega_q)\tau})_{q-p}}{i\omega_q + i\omega_p + l - \sigma_{HH} s_1 (J e^{-i(\omega_p + \omega_q)\tau})_{q-p}} \right) \right]$$

where $(J e^{-i\omega_p \tau_{HH}})_p = \frac{i\omega_p + l}{\sigma_{HH} s_1}$, $(J e^{-i\omega_q \tau_{HH}})_q = \frac{i\omega_q + l}{\sigma_{HH} s_1}$ and $s_2 \equiv S_0^{(2)}(0)$, $s_3 \equiv S_0^{(3)}(0)$.

Proof. We start with the expression of the eigenvectors:

$$\phi_1 = \begin{bmatrix} e_p \\ e^{i\omega_p \theta} e_p \end{bmatrix}, \quad \phi_2 = \begin{bmatrix} e_{-p} \\ e^{i\omega_p \theta} e_{-p} \end{bmatrix}, \quad \phi_3 = \begin{bmatrix} e_q \\ e^{i\omega_q \theta} e_q \end{bmatrix}, \quad \phi_4 = \begin{bmatrix} e_{-q} \\ e^{i\omega_q \theta} e_{-q} \end{bmatrix}$$

and that the associated vectors for the spectral projector (25):

$$\psi_1 = \beta_1 \begin{bmatrix} e_p \\ e^{-i\omega_p \theta} e_p \end{bmatrix}, \quad \psi_2 = \beta_1 \begin{bmatrix} e_{-p} \\ e^{-i\omega_p \theta} e_{-p} \end{bmatrix}, \quad \psi_3 = \beta_2 \begin{bmatrix} e_q \\ e^{-i\omega_q \theta} e_q \end{bmatrix}, \quad \psi_4 = \beta_2 \begin{bmatrix} e_{-q} \\ e^{-i\omega_q \theta} e_{-q} \end{bmatrix}.$$

Using the same procedure as for computation of the previous normal forms in the coordinates system $v_0 = z_1 \phi_1 + z_2 \phi_2 + z_3 \phi_3 + z_4 \phi_4 + c.c.$, we find the next equations.

$$-6\mathbf{R}_3(\phi_1, \phi_3, \overline{\phi_3}) - 2\mathbf{R}_2(\tilde{\Psi}_{1,0,0,0,0,1,0,0,0}, \phi_3) - 2\mathbf{R}_2(\overline{\phi_3}, \tilde{\Psi}_{1,0,0,0,0,1,0,0,0}) + (i\omega_l - \mathbf{A}) \tilde{\Psi}_{1,0,0,0,1,1,0,0,0} \\ - 2\mathbf{R}_2(\phi_1, \tilde{\Psi}_{0,0,0,0,1,1,0,0,0}) + d_{(1)}^{(HH)} \phi_1 = 0$$

$$-6\mathbf{R}_3(\phi_1 \phi_4 \overline{\phi_4}) - 2\mathbf{R}_2(\phi_1 \tilde{\Psi}_{0,0,0,0,0,0,1,1,0}) + (i\omega_l - \mathbf{A}) \tilde{\Psi}_{1,0,0,0,0,0,1,1,0} - 2\mathbf{R}_2(\tilde{\Psi}_{1,0,0,0,0,0,0,1,0} \phi_4) \\ - 2\mathbf{R}_2(\overline{\phi_4} \tilde{\Psi}_{1,0,0,0,0,0,1,0,0}) + e_{(1)}^{(HH)} \phi_1 = 0$$

$$-2\mathbf{R}_2(\tilde{\Psi}_{0,1,0,0,1,0,0,0,0}, \phi_1) - 2\mathbf{R}_2(\overline{\phi_1}, \tilde{\Psi}_{1,0,0,0,1,0,0,0,0}) + (i\omega_m - \mathbf{A}) \tilde{\Psi}_{1,1,0,0,1,0,0,0,0} - 6\mathbf{R}_3(\phi_1 \phi_3 \overline{\phi_1}) \\ - 2\mathbf{R}_2(\phi_3 \tilde{\Psi}_{1,1,0,0,0,0,0,0,0}) + b_{(3)}^{(HH)} \phi_3 = 0$$

$$-2\mathbf{R}_2(\phi_3 \tilde{\Psi}_{0,0,1,1,0,0,0,0,0}) - 6\mathbf{R}_3(\phi_3, \phi_2, \overline{\phi_2}) - 2\mathbf{R}_2(\tilde{\Psi}_{0,0,0,1,1,0,0,0,0}, \phi_2) - 2\mathbf{R}_2(\overline{\phi_2}, \tilde{\Psi}_{0,0,1,0,1,0,0,0,0}) \\ + (i\omega_m - \mathbf{A}) \tilde{\Psi}_{0,0,1,1,1,0,0,0,0} + c_{(3)}^{(HH)} \phi_3 = 0$$

which gives (using the spectral projector):

$$\begin{aligned} \langle\langle \bar{\psi}_1, 6\mathbf{R}_3(\phi_1, \phi_3, \bar{\phi}_3) + 2\mathbf{R}_2(\tilde{\Psi}_{1,0,0,0,0,1,0,0,0}, \phi_3) + 2\mathbf{R}_2(\bar{\phi}_3, \tilde{\Psi}_{1,0,0,0,0,1,0,0,0,0}) + 2\mathbf{R}_2(\phi_1, \tilde{\Psi}_{0,0,0,0,1,1,0,0,0}) \rangle\rangle &= d \\ \langle\langle \bar{\psi}_1, 6\mathbf{R}_3(\phi_1, \phi_4, \bar{\phi}_4) + 2\mathbf{R}_2(\phi_1, \tilde{\Psi}_{0,0,0,0,0,0,1,1,0}) + 2\mathbf{R}_2(\tilde{\Psi}_{1,0,0,0,0,0,0,1,0}, \phi_4) + 2\mathbf{R}_2(\bar{\phi}_4, \tilde{\Psi}_{1,0,0,0,0,0,1,0,0}) \rangle\rangle &= e \\ \langle\langle \bar{\psi}_3, 6\mathbf{R}_3(\phi_1, \phi_3, \bar{\phi}_1) + 2\mathbf{R}_2(\tilde{\Psi}_{0,1,0,0,1,0,0,0,0}, \phi_1) + 2\mathbf{R}_2(\bar{\phi}_1, \tilde{\Psi}_{1,0,0,0,0,1,0,0,0}) + 2\mathbf{R}_2(\phi_3, \tilde{\Psi}_{1,1,0,0,0,0,0,0,0}) \rangle\rangle &= b \\ \langle\langle \bar{\psi}_3, 6\mathbf{R}_3(\phi_3, \phi_2, \bar{\phi}_2) + 2\mathbf{R}_2(\phi_3, \tilde{\Psi}_{0,0,1,1,0,0,0,0,0}) + 2\mathbf{R}_2(\tilde{\Psi}_{0,0,0,1,1,0,0,0,0}, \phi_2) + 2\mathbf{R}_2(\bar{\phi}_2, \tilde{\Psi}_{0,0,1,0,1,0,0,0,0}) \rangle\rangle &= c \end{aligned}$$

I.1 Equations needed for $d_{(1)}^{(HH)}$

We find:

$$\begin{aligned} (-i\omega_q + i\omega_p - \mathbf{A}) \tilde{\Psi}_{1,0,0,0,0,1,0,0,0} &= 2\mathbf{R}_2(\bar{\phi}_3, \phi_1) = \sigma_{HH}^2 s_2 \left(J e^{-i(\omega_p - \omega_q)\tau} \right)_{p-q} \begin{bmatrix} e_{p-q} \\ 0 \end{bmatrix} \\ (i\omega_p + i\omega_q - \mathbf{A}) \tilde{\Psi}_{1,0,0,0,0,1,0,0,0} &= 2\mathbf{R}_2(\phi_3, \phi_1) = \sigma_{HH}^2 s_2 \left(J e^{-i(\omega_p + \omega_q)\tau} \right)_{p+q} \begin{bmatrix} e_{p+q} \\ 0 \end{bmatrix} \\ \mathbf{A} \tilde{\Psi}_{0,0,0,0,1,1,0,0,0} &= -2\mathbf{R}_2(\bar{\phi}_3, \phi_3) = -\sigma_{HH}^2 s_2 J_0 \begin{bmatrix} e_0 \\ 0 \end{bmatrix} \end{aligned}$$

which gives

$$\begin{aligned} \tilde{\Psi}_{1,0,0,0,0,1,0,0,0} &= \frac{\sigma_{HH}^2 s_2 \left(J e^{-i(\omega_p - \omega_q)\tau} \right)_{p-q}}{-i\omega_q + i\omega_p + l - \sigma_{HH} s_1 \left(J e^{-i(\omega_p - \omega_q)\tau} \right)_{p-q}} e_{p-q} e^{i(\omega_p - \omega_q)\theta} \\ \tilde{\Psi}_{1,0,0,0,0,1,0,0,0} &= \frac{\sigma_{HH}^2 s_2 \left(J e^{-i(\omega_p + \omega_q)\tau} \right)_{p+q}}{i\omega_q + i\omega_p + l - \sigma_{HH} s_1 \left(J e^{-i(\omega_p + \omega_q)\tau} \right)_{p+q}} e_{p+q} e^{i(\omega_p + \omega_q)\theta} \\ \tilde{\Psi}_{0,0,0,0,1,1,0,0,0} &= \frac{\sigma_{HH}^2 s_2 J_0}{l - s_1 \sigma_{HH} J_0} e_0 \end{aligned}$$

I.2 Equations needed for $e_{(1)}^{(HH)}$

We find:

$$\begin{aligned} \mathbf{A} \tilde{\Psi}_{0,0,0,0,0,0,1,1,0} &= -2\mathbf{R}_2(\bar{\phi}_4, \phi_4) = -\sigma_{HH}^2 s_2 J_0 \begin{bmatrix} e_0 \\ 0 \end{bmatrix} \\ (i\omega_p - i\omega_q - \mathbf{A}) \tilde{\Psi}_{1,0,0,0,0,0,0,1,0} &= 2\mathbf{R}_2(\bar{\phi}_4, \phi_1) = \sigma_{HH}^2 s_2 \left(J e^{-i(\omega_p - \omega_q)\tau} \right)_{p+q} \begin{bmatrix} e_{p+q} \\ 0 \end{bmatrix} \\ (i\omega_p + i\omega_q - \mathbf{A}) \tilde{\Psi}_{1,0,0,0,0,0,0,1,0} &= 2\mathbf{R}_2(\phi_4, \phi_1) = \sigma_{HH}^2 s_2 \left(J e^{-i(\omega_p + \omega_q)\tau} \right)_{p-q} \begin{bmatrix} e_{p-q} \\ 0 \end{bmatrix} \end{aligned}$$

which gives:

$$\begin{aligned} \tilde{\Psi}_{0,0,0,0,0,0,1,1,0} &= \frac{\sigma_{HH}^2 s_2 J_0}{l - s_1 \sigma_{HH} J_0} e_0 \\ \tilde{\Psi}_{1,0,0,0,0,0,0,1,0} &= \frac{\sigma_{HH}^2 s_2 \left(J e^{-i(\omega_p - \omega_q)\tau} \right)_{p+q}}{i\omega_p - i\omega_q + l - \sigma_{HH} s_1 \left(J e^{-i(\omega_p - \omega_q)\tau} \right)_{p+q}} e_{p+q} e^{i(\omega_p - \omega_q)\theta} \\ \tilde{\Psi}_{1,0,0,0,0,0,0,1,0} &= \frac{\sigma_{HH}^2 s_2 \left(J e^{-i(\omega_p + \omega_q)\tau} \right)_{p-q}}{i\omega_q + i\omega_p + l - \sigma_{HH} s_1 \left(J e^{-i(\omega_p + \omega_q)\tau} \right)_{p-q}} e_{p-q} e^{i(\omega_p + \omega_q)\theta} \end{aligned}$$

I.3 Equations needed for $b_{(3)}^{(HH)}$

We find:

$$\begin{aligned} (i\omega_q - i\omega_p - \mathbf{A}) \tilde{\Psi}_{0,1,0,0,1,0,0,0,0} &= 2\mathbf{R}_2(\phi_3, \overline{\phi_1}) = \sigma_{HH}^2 s_2 \left(J e^{-i(\omega_q - \omega_p)\tau} \right)_{q-p} \begin{bmatrix} e_{q-p} \\ 0 \end{bmatrix} \\ (i\omega_q + i\omega_p - \mathbf{A}) \tilde{\Psi}_{1,0,0,0,1,0,0,0,0} &= 2\mathbf{R}_2(\phi_3, \phi_1) = \sigma_{HH}^2 s_2 \left(J e^{-i(\omega_q + \omega_p)\tau} \right)_{q+p} \begin{bmatrix} e_{q+p} \\ 0 \end{bmatrix} \\ \mathbf{A} \tilde{\Psi}_{1,1,0,0,0,0,0,0,0} &= -2\mathbf{R}_2(\overline{\phi_1}, \phi_1) = -\sigma_{HH}^2 s_2 J_0 \begin{bmatrix} e_0 \\ 0 \end{bmatrix} \end{aligned}$$

which gives:

$$\begin{aligned} \tilde{\Psi}_{0,1,0,0,1,0,0,0,0} &= \frac{\sigma_{HH}^2 s_2 \left(J e^{-i(\omega_q - \omega_p)\tau} \right)_{q-p}}{i\omega_q - i\omega_p + l - \sigma_{HH} s_1 \left(J e^{-i(\omega_q - \omega_p)\tau} \right)_{q-p}} e_{q-p} e^{i(\omega_q - \omega_p)\theta} \\ \tilde{\Psi}_{1,0,0,0,1,0,0,0,0} &= \frac{\sigma_{HH}^2 s_2 \left(J e^{-i(\omega_p + \omega_q)\tau} \right)_{p+q}}{i\omega_q + i\omega_p + l - \sigma_{HH} s_1 \left(J e^{-i(\omega_p + \omega_q)\tau} \right)_{p+q}} e_{p+q} e^{i(\omega_p + \omega_q)\theta} \\ \tilde{\Psi}_{1,1,0,0,0,0,0,0,0} &= \frac{\sigma_{HH}^2 s_2 J_0}{l - s_1 \sigma_{HH} J_0} e_0 \end{aligned}$$

I.4 Equations needed for $c_{(3)}^{(HH)}$

We find:

$$\begin{aligned} (-i\omega_p + i\omega_q - \mathbf{A}) \tilde{\Psi}_{0,0,0,1,1,0,0,0,0} &= 2\mathbf{R}_2(\phi_3, \overline{\phi_2}) = \sigma_{HH}^2 s_2 \left(J e^{-i(\omega_q - \omega_p)\tau} \right)_{p+q} \begin{bmatrix} e_{p+q} \\ 0 \end{bmatrix} \\ (i\omega_q + i\omega_p - \mathbf{A}) \tilde{\Psi}_{0,0,1,0,1,0,0,0,0} &= 2\mathbf{R}_2(\phi_3, \phi_2) = \sigma_{HH}^2 s_2 \left(J e^{-i(\omega_q + \omega_p)\tau} \right)_{q-p} \begin{bmatrix} e_{q-p} \\ 0 \end{bmatrix} \\ \mathbf{A} \tilde{\Psi}_{0,0,1,1,0,0,0,0,0} &= -2\mathbf{R}_2(\overline{\phi_2}, \phi_2) = -2\mathbf{R}_2(\overline{\phi_1}, \phi_1) = -\sigma_{HH}^2 s_2 J_0 \begin{bmatrix} e_0 \\ 0 \end{bmatrix} \end{aligned}$$

which gives:

$$\begin{aligned} \tilde{\Psi}_{0,0,0,1,1,0,0,0,0} &= \frac{\sigma_{HH}^2 s_2 \left(J e^{-i(\omega_q - \omega_p)\tau} \right)_{q+p}}{i\omega_q - i\omega_p + l - \sigma_{HH} s_1 \left(J e^{-i(\omega_q - \omega_p)\tau} \right)_{p+q}} e_{p+q} e^{i(\omega_q - \omega_p)\theta} \\ \tilde{\Psi}_{0,0,1,0,1,0,0,0,0} &= \frac{\sigma_{HH}^2 s_2 \left(J e^{-i(\omega_p + \omega_q)\tau} \right)_{q-p}}{i\omega_q + i\omega_p + l - \sigma_{HH} s_1 \left(J e^{-i(\omega_p + \omega_q)\tau} \right)_{m-l}} e_{m-l} e^{i(\omega_p + \omega_q)\theta} \\ \tilde{\Psi}_{0,0,1,1,0,0,0,0,0} &= \frac{\sigma_{HH}^2 s_2 J_0}{l - s_1 \sigma_{HH} J_0} e_0 \end{aligned}$$

Contents

1 Introduction	3
2 The neural field model	4
3 Mathematical framework and notations	6

4	Linear analysis	7
4.1	Hopf curve in the case of constant delays $c = 0$	8
4.2	Hopf curve in the case of space dependent delays	8
5	Nonlinear analysis, normal form computation	10
5.1	Scaling of parameters	11
5.2	The Pitchfork bifurcation	11
5.3	The $O(2)$ -Hopf bifurcation	11
5.4	The Pitchfork-Hopf normal form	12
5.5	The Hopf-Hopf normal form	13
5.6	Six-dimensional case	14
5.7	Eight-dimensional case	16
6	Application to two types of connectivity functions	16
6.1	Mexican-hat connectivity	17
6.1.1	Constant delays	17
6.1.2	Space dependent delays	18
6.2	Inverted Mexican-hat connectivity	19
6.2.1	Constant delays	19
6.2.2	Space dependent delays	21
6.2.3	Six dimensional Hopf-Hopf bifurcations	22
6.2.4	Eight dimensional Hopf-Hopf bifurcations	23
6.2.5	Symmetry breaking effects	25
7	Discussion and conclusion	26
A	Numerical tools	28
B	Cauchy problem	29
C	Normal form computation	30
D	Spectral projector	31
E	The Pitchfork bifurcation	32
F	The $O(2)$-Hopf bifurcation	33
G	Pitchfork-Hopf bifurcation	34
H	Hopf-Hopf normal form, 6d case	36
I	Hopf-Hopf normal form, 8d case	38
I.1	Equations needed for $d_{(1)}^{(HH)}$	40
I.2	Equations needed for $e_{(1)}^{(HH)}$	40
I.3	Equations needed for $b_{(3)}^{(HH)}$	41
I.4	Equations needed for $c_{(3)}^{(HH)}$	41

References

- [AH05] Fatihcan M. Atay and Axel Hutt. Stability and bifurcations in neural fields with finite propagation speed and general connectivity. *SIAM Journal on Applied Mathematics*, 65(2):644–666, 2005.
- [AH06] Fatihcan M. Atay and Axel Hutt. Neural fields with distributed transmission speeds and long-range feedback delays. *SIAM Journal of Applied Dynamical Systems*, 5(4):670–698, 2006.
- [Ama77] S.-I. Amari. Dynamics of pattern formation in lateral-inhibition type neural fields. *Biological Cybernetics*, 27(2):77–87, June 1977.
- [BBC00] P.C. Bressloff, N.W. Bressloff, and J.D. Cowan. Dynamical mechanism for sharp orientation tuning in an integrate-and-fire model of a cortical hypercolumn. *Neural computation*, 12(11):2473–2511, 2000.
- [BC94] J. Bélair and S.A. Campbell. Stability and bifurcations of equilibria in a multiple-delayed differential equation. *SIAM Journal on Applied Mathematics*, pages 1402–1424, 1994.
- [BCG⁺01] P.C. Bressloff, J.D. Cowan, M. Golubitsky, P.J. Thomas, and M.C. Wiener. Geometric visual hallucinations, euclidean symmetry and the functional architecture of striate cortex. *Phil. Trans. R. Soc. Lond. B*, 306(1407):299–330, March 2001.
- [BCVDD96] J. Bélair, S.A. Campbell, and P. Van Den Driessche. Frustration, stability, and delay-induced oscillations in a neural network model. *SIAM Journal on Applied Mathematics*, pages 245–255, 1996.
- [BK08] P.C. Bressloff and Z.P. Kilpatrick. Nonlocal ginzburg-landau equation for cortical pattern formation. *Physical Review E*, 78(4):41916:1–16, 2008.
- [BKF⁺10] J.M.L. Budd, K. Kovács, A.S. Ferecskó, P. Buzás, U.T. Eysel, and Z.F. Kisvárdy. Neocortical axon arbors trade-off material and conduction delay conservation. *PLoS Comput Biol*, 6(3):e1000711, 2010.
- [BL10] I. Bojak and D.T.J. Liley. Axonal velocity distributions in neural field equations. *PLOS Comp. Bio.*, 2010.
- [Bre03] P.C. Bressloff. Spatially periodic modulation of cortical patterns by long-range horizontal connections. *Physica D: Nonlinear Phenomena*, 185(3-4):131–157, 2003.
- [BYBOS95] R. Ben-Yishai, RL Bar-Or, and H. Sompolinsky. Theory of orientation tuning in visual cortex. *Proceedings of the National Academy of Sciences*, 92(9):3844–3848, 1995.
- [CE04] R. Curtu and B. Ermentrout. Pattern formation in a network of excitatory and inhibitory cells with adaptation. *SIAM Journal on Applied Dynamical Systems*, 3:191, 2004.
- [CGH⁺96] R.M. Corless, G.H. Gonnet, D.E.G. Hare, D.J. Jeffrey, and D.E. Knuth. On the lambertw function. *Advances in Computational mathematics*, 5(1):329–359, 1996.
- [CGK86] P. Chossat, M. Golubitsky, and B.L. Keyfitz. Hopf-hopf mode interactions with o(2) symmetry. *Dynamical Systems*, 1(4):255–292, 1986.

- [CL00] P. Chossat and R. Lauterbach. *Methods in Equivariant Bifurcations and Dynamical Systems*. World Scientific Publishing Company, 2000.
- [CL09] S. Coombes and C. Laing. Delays in activity based neural networks. *Philosophical Transactions of the Royal Society A.*, 367:1117–1129, 2009.
- [Coo05] Stephen Coombes. Waves, bumps, and patterns in neural fields theories. *Biological Cybernetics*, 93(2):91–108, 2005.
- [CVS⁺07] S. Coombes, N.A Venkov, L. Shiau, I. Bojak, D.T.J. Liley, and C.R. Laing. Modeling electrocortical activity through local approximations of integral neural field equations. *Physical Review E*, 76(5):51901, 2007.
- [CY08] S.A. Campbell and Y. Yuan. Zero singularities of codimension two and three in delay differential equations. *Nonlinearity*, 21:2671, 2008.
- [CYB05] S.A. Campbell, Y. Yuan, and S.D. Bungay. Equivariant hopf bifurcation in a ring of identical cells with delayed coupling. *Nonlinearity*, 18:2827, 2005.
- [Die95] O. Diekmann. *Delay equations: functional-, complex-, and nonlinear analysis*. Springer, 1995.
- [DK91] G. Dangelmayr and E. Knobloch. Hopf bifurcation with broken circular symmetry. *Nonlinearity*, 4:399, 1991.
- [EC79] GB Ermentrout and J.D. Cowan. Temporal oscillations in neuronal nets. *Journal of mathematical biology*, 7(3):265–280, 1979.
- [EC80] G.B. Ermentrout and J.D. Cowan. Large scale spatially organized activity in neural nets. *SIAM Journal on Applied Mathematics*, pages 1–21, 1980.
- [Erm98] Bard Ermentrout. Neural networks as spatio-temporal pattern-forming systems. *Reports on Progress in Physics*, 61:353–430, 1998.
- [FGS08] O. Faugeras, F. Grimbert, and J.-J. Slotine. Absolute stability and complete synchronization in a class of neural fields models. *SIAM Journal of Applied Mathematics*, 61(1):205–250, September 2008.
- [GH83] J. Guckenheimer and P. J. Holmes. *Nonlinear Oscillations, Dynamical Systems and Bifurcations of Vector Fields*, volume 42 of *Applied mathematical sciences*. Springer, 1983.
- [GS84] M. Golubitsky and D.G. Schaeffer. *Singularities and Groups in Bifurcation Theory*, volume I. Springer, 1984.
- [GS85] M. Golubitsky and I. Stewart. Hopf bifurcation in the presence of symmetry. *Archive for Rational Mechanics and Analysis*, 87(2):107–165, 1985.
- [GSS88] M. Golubitsky, I. Stewart, and D.G. Schaeffer. *Singularities and Groups in Bifurcation Theory*, volume II. Springer, 1988.
- [HA06] A. Hutt and F.M. Atay. Effects of distributed transmission speeds on propagating activity in neural populations. *Physical Review E*, 73(021906):1–5, 2006.

- [HH52] A.L. Hodgkin and A.F. Huxley. A quantitative description of membrane current and its application to conduction and excitation in nerve. *Journal of Physiology*, 117:500–544, 1952.
- [HI10] M. Haragus and G. Iooss. *Local bifurcations, center manifolds, and normal forms in infinite dimensional systems*. EDP Sci. Springer Verlag UTX series, 2010.
- [HL93] J.K. Hale and S.M.V. Lunel. *Introduction to functional differential equations*. Springer Verlag, 1993.
- [HR10] A. Hutt and N. Rougier. Activity spread and breathers induced by finite transmission speeds in two-dimensional neural fields. *Physical Review E*, 82(5):055701, 2010.
- [Hut08] A. Hutt. Local excitation-lateral inhibition interaction yields oscillatory instabilities in nonlocally interacting systems involving finite propagation delays. *Physics Letters A*, 372:541–546, 2008.
- [Hut09] A. Hutt. Finite propagation speeds in spatially extended systems. *Complex Time-Delay Systems: Theory and Applications*, page 151, 2009.
- [JK00] VK Jirsa and JAS Kelso. Spatiotemporal pattern formation in neural systems with heterogeneous connection topologies. *Physical Review E*, 62(6):8462–8465, 2000.
- [Kuz98] Yuri A. Kuznetsov. *Elements of Applied Bifurcation Theory*. Applied Mathematical Sciences. Springer, 2nd edition, 1998.
- [LAB03] Jennifer S. Lund, Alessandra Angelucci, and Paul C. Bressloff. Anatomical substrates for functional columns in macaque monkey primary visual cortex. *Cerebral Cortex*, 12:15–24, 2003.
- [LI80] W.-F. Langford and G. Iooss. Interactions of hopf and pitchfork bifurcations. *Bifurcation Problems and their Numerical Solution*. HD Mittelman and H. Weber editors, ISNM, 54:103–134, 1980.
- [MIGJ10] V. Markounikau, C. Igel, A. Grinvald, and D. Jancke. A dynamic neural field model of mesoscopic cortical activity captured with voltage-sensitive dye imaging. *PLoS Comput Biol*, 6(9):e1000919, 2010.
- [PBS⁺96] D.J. Pinto, J.C. Brumberg, D.J. Simons, G.B. Ermentrout, and R. Traub. A quantitative population model of whisker barrels: re-examining the wilson-cowan equations. *Journal of Computational Neuroscience*, 3(3):247–264, 1996.
- [RBH05] A. Roxin, N. Brunel, and D. Hansel. Role of Delays in Shaping Spatiotemporal Dynamics of Neuronal Activity in Large Networks. *Physical Review Letters*, 94(23):238103, 2005.
- [RM11] A. Roxin and E. Montbrió. How effective delays shape oscillatory dynamics in neuronal networks. *Physica. D*, 240(3):323–345, 2011.
- [SC00] L.P. Shayer and S.A. Campbell. Stability, bifurcation, and multistability in a system of two coupled neurons with multiple time delays. *SIAM Journal on Applied Mathematics*, 61(2):673–700, 2000.

- [SHD04] Marzio Sala, Michael A. Heroux, and David M. Day. Trilinos tutorial. Technical Report SAND2004-2189, Sandia National Laboratories, 2004.
- [ST01] L.F. Shampine and S. Thompson. Solving ddes in matlab. *Applied Numerical Mathematics*, 37:441–458, 2001.
- [Tou12] Jonathan Touboul. Mean-field equations for stochastic firing-rate neural fields with delays: Derivation and noise-induced transitions. *Physica D: Nonlinear Phenomena*, 241(15):1223–1244, August 2012.
- [VCM07] N.A. Venkov, S. Coombes, and P.C. Matthews. Dynamic instabilities in scalar neural field equations with space-dependent delays. *Physica D: Nonlinear Phenomena*, 232:1–15, 2007.
- [Vel11] Romain Veltz. An analytical method for computing hopf bifurcation curves in neural field networks with space-dependent delays. *Comptes Rendus Mathematique*, 349:749–752, July 2011.
- [VF10] Romain Veltz and Olivier Faugeras. Local/global analysis of the stationary solutions of some neural field equations. *SIAM Journal on Applied Dynamical Systems*, 9(3):954–998, August 2010.
- [VF11] Romain Veltz and Olivier Faugeras. Stability of the stationary solutions of neural field equations with propagation delays. *The Journal of Mathematical Neuroscience*, 1(1):1, 2011.
- [VF12] Romain Veltz and Olivier Faugeras. A center manifold result for delayed neural fields equations. *SIAM Journal on Applied Mathematics (Submitted)*, July 2012.
- [VI92] A. Vanderbauwhede and G. Iooss. Center manifold theory in infinite dimensions. *Dynamics Reported PJ-Expositions in Dynamical Systems. Vol. 1, New Series. Springer-Verlag, Berlin*, page 125, 1992.
- [WC73] H.R. Wilson and J.D. Cowan. A mathematical theory of the functional dynamics of cortical and thalamic nervous tissue. *Biological Cybernetics*, 13(2):55–80, September 1973.
- [Wu98] J. Wu. Symmetric functional differential equations and neural networks with memory. *Transactions of the American Mathematical Society*, 350(12):4799–4838, 1998.
- [Wu01] J. Wu. *Introduction to neural dynamics and signal transmission delay*. Walter de Gruyter, 2001.



**RESEARCH CENTRE
SOPHIA ANTIPOLIS – MÉDITERRANÉE**

2004 route des Lucioles - BP 93
06902 Sophia Antipolis Cedex

Publisher
Inria
Domaine de Voluceau - Rocquencourt
BP 105 - 78153 Le Chesnay Cedex
inria.fr

ISSN 0249-6399